HHS Public Access

Author manuscript

Neuroimage. Author manuscript; available in PMC 2023 May 15.

Published in final edited form as:

Neuroimage. 2023 May 15; 272: 120060. doi:10.1016/j.neuroimage.2023.120060.

The psychosis human connectome project: Design and rationale for studies of visual neurophysiology

Michael-Paul Schallmo[a,*], **Kimberly B. Weldon**[b,a], **Rohit S. Kamath**[a], **Hannah R. Moser**[a], **Samantha A. Montoya**[a], **Kyle W. Killebrew**[a], **Caroline Demro**[a,d], **Andrea N. Grant**[b], **Małgorzata Marjańska**[b], **Scott R. Sponheim**[c,a], **Cheryl A. Olman**[d,b]

[a]Department of Psychiatry and Behavioral Sciences, University of Minnesota, Minneapolis, MN, USA

[b]Department of Radiology, Center for Magnetic Resonance Research, University of Minnesota, Minneapolis, MN, USA

[c]Veterans Affairs Medical Center, Minneapolis, MN, USA

[d]Department of Psychology, University of Minnesota, Minneapolis, MN, USA

Abstract

Visual perception is abnormal in psychotic disorders such as schizophrenia. In addition to hallucinations, laboratory tests show differences in fundamental visual processes including contrast sensitivity, center-surround interactions, and perceptual organization. A number of hypotheses have been proposed to explain visual dysfunction in psychotic disorders, including an imbalance between excitation and inhibition. However, the precise neural basis of abnormal visual perception in people with psychotic psychopathology (PwPP) remains unknown. Here, we describe the behavioral and 7 tesla MRI methods we used to interrogate visual neurophysiology in PwPP as part of the Psychosis Human Connectome Project (HCP). In addition to PwPP (n = 66) and healthy controls (n = 43), we also recruited first-degree biological relatives (n = 44) in order to examine the role of genetic liability for psychosis in visual perception. Our visual tasks were designed to assess fundamental visual processes in PwPP, whereas MR spectroscopy

*Corresponding author. schal110@umn.edu (M.-P. Schallmo).

Declaration of Competing Interest

The authors declare that they have no conflicts of interest regarding the publication of this manuscript. None.

Credit authorship contribution statement

Michael-Paul Schallmo: Conceptualization, Methodology, Software, Formal analysis, Investigation, Data curation, Visualization, Supervision, Project administration, Writing – original draft, Writing – review & editing. **Kimberly B. Weldon:** Formal analysis, Investigation, Visualization, Writing – review & editing. **Rohit S. Kamath:** Formal analysis, Investigation, Visualization, Writing – review & editing. **Hannah R. Moser:** Data curation, Formal analysis, Investigation, Writing – review & editing. **Samantha A. Montoya:** Formal analysis, Investigation, Visualization, Writing – review & editing. **Kyle W. Killebrew:** Formal analysis, Investigation, Visualization, Writing – review & editing. **Caroline Demro:** Formal analysis, Writing – review & editing. **Andrea N. Grant:** Methodology, Software, Investigation, Writing – review & editing. **Małgorzata Marjańska:** Conceptualization, Methodology, Software, Resources, Supervision, Funding acquisition, Writing – review & editing. **Scott R. Sponheim:** Conceptualization, Methodology, Resources, Supervision, Project administration, Funding acquisition, Writing – review & editing. **Cheryl A. Olman:** Conceptualization, Methodology, Software, Formal analysis, Investigation, Resources, Data curation, Visualization, Supervision, Project administration, Funding acquisition, Writing – original draft, Writing – review & editing.

Supplementary materials

Supplementary material associated with this article can be found, in the online version, at doi:10.1016/j.neuroimage.2023.120060.

enabled us to examine neurochemistry, including excitatory and inhibitory markers. We show that it is feasible to collect high-quality data across multiple psychophysical, functional MRI, and MR spectroscopy experiments with a sizable number of participants at a single research site. These data, in addition to those from our previously described 3 tesla experiments, will be made publicly available in order to facilitate further investigations by other research groups. By combining visual neuroscience techniques and HCP brain imaging methods, our experiments offer new opportunities to investigate the neural basis of abnormal visual perception in PwPP.

Keywords

7 tesla; Task fMRI; MR spectroscopy; Schizophrenia; Bipolar disorder; Biological relatives

1. Introduction and background

Abnormal visual perception is a symptom of psychosis spectrum disorders (e.g., schizophrenia), and includes both frank hallucinations and distorted perception of actual stimuli. The point prevalence of visual hallucinations in schizophrenia is 27%, and such anomalies are associated with greater disease severity and poorer outcomes (Waters et al., 2014). Laboratory assessments of visual perception have also shown more subtle abnormalities in people with psychotic psychopathology (for reviews, see Butler et al. 2008; King et al. 2017; Klein et al. 2020a; Notredame et al. 2014; Phillips and Silverstein 2013; Yoon et al. 2013). While much is known about the neural mechanisms of visual perception in healthy individuals, it is not yet clear what differences in neural processing underlie visual dysfunction in people with psychotic psychopathology (PwPP), which limits the development of more effective treatment strategies for psychotic illness (e.g., to improve sensory functioning). A number of hypotheses have been proposed to explain visual disturbances in PwPP, including a disrupted balance of excitation and inhibition (Foss-Feig et al., 2017; Lewis et al., 2005; Lisman, 2012; Moghaddam and Javitt, 2012), thalamo-cortical dysconnectivity (Anticevic et al., 2014; Cheng et al., 2015; Damaraju et al., 2014; Dong et al., 2019; Giraldo-Chica and Woodward, 2017; Ramsay, 2019; Ramsay et al., 2017), abnormal visual gain control (Butler et al., 2008; Phillips and Silverstein, 2013), impaired top-down attentional processing (Gold et al., 2018; Luck et al., 2019a; Luck et al., 2019b), and disrupted predictive coding (Adams et al., 2013; Horga and Abi-Dargham, 2019; Sterzer et al., 2018). The current study was designed to provide a publicly available, multimodal neuroimaging data set to facilitate testing these (and other) hypotheses regarding the nature of visual dysfunction among PwPP.

Beyond the relevance to hallucinations and perceptual distortions, there is additional motivation for studying visual functioning among PwPP, as the visual system offers a strong translational bridge between basic neuroscience in animal models and studies in humans with psychosis. Basic neuroscience research in animal models has provided a detailed knowledge of how neural functions are linked to perception. There is significant homology between the visual systems of well-studied animal models (e.g., cats, ferrets, and non-human primates) and humans (Hubel and Wiesel, 1962; Van Essen et al., 1992). It is also relatively straightforward to adapt visual paradigms from animal models for use in human studies, and

vice versa. This allows investigators to make strong inferences about the neurophysiological basis of perceptual anomalies seen in PwPP, which may be challenging when studying higher-order cognitive functions. In this study, we used visual paradigms designed to tap into several different aspects or levels of visual functioning. We provide further details on the background and motivation for the specific paradigms that we chose for this study in the Supplemental Information.

Several theories have been offered regarding the physiological basis of impaired visual perception in psychosis spectrum disorders, including an imbalance between excitation and inhibition (E/I) within visual brain regions, which may depend on excess excitation, reduced inhibition, or both (Foss-Feig et al., 2017; Lisman, 2012). The idea of E/I imbalance has the advantage of merging two neurochemical theories of schizophrenia (or psychotic disorders more generally) that have received widespread attention and support: the glutamate hypothesis (Javitt, 2004; Moghaddam and Javitt, 2012) and the γ-aminobutyric acid (GABA) hypothesis (Gonzalez-Burgos and Lewis, 2008; Hashimoto et al., 2008; Lewis et al., 2005). ^{1}H magnetic resonance spectroscopy (MRS) is a popular method for investigating neurochemistry noninvasively in the human brain, and can be used to measure concentrations of various metabolites, including excitatory (i.e., glutamate) and inhibitory (i.e., GABA) neurotransmitters (Mescher et al., 1998; Tkáč et al., 2001). Previous MRS studies have offered somewhat mixed support for group differences in these metabolites within visual regions in PwPP (Sydnor and Roalf, 2020; Taylor and Tso, 2015), with some suggesting abnormal glutamate and / or GABA levels in visual cortex among PwPP (Kelemen et al., 2013; Thakkar et al., 2017; Yoon et al., 2020, 2010), and others reporting no differences versus controls (Kumar et al., 2020; Marsman et al., 2014).

There are some important methodological considerations for MR spectroscopy studies in PwPP, including the challenge of separating signals from neurochemicals of interest from those attributable to macromolecules (Cudalbu et al., 2021). In schizophrenia, faster metabolite transverse relaxation time constants (T_2) have also been reported (Öngür et al., 2010a). This raises the possibility that reports of lower metabolite concentrations among PwPP (versus controls) in MRS studies using sequences with longer echo times (TEs) might reflect a difference in T_2, rather than true group differences in metabolite concentrations. Here, we used an ultra-short (8 ms) TE STEAM sequence (Marjańska et al., 2017; Tkáč et al., 2001), in order to address the potentially confounding effects of shorter T_2 in PwPP in future studies using these data. We also plan to explicitly account for the contribution of macromolecules within our spectra based on measurements from inversion-recovery experiments (Marjańska et al., 2017) in future analyses of these data.

Another important factor for understanding the neurobiology of visual dysfunction among PwPP is genetics. Genetic factors play an important role in the development of psychotic disorders (Cardno et al., 1999; Cardno and Owen, 2014), but the link between genetic liability for psychotic illness and disordered visual perception remains unclear. Studying the first-degree biological relatives of PwPP (i.e., parents, siblings or children, who share on average 50% of their genes) may provide insight into the genetic basis of visual processing abnormalities in psychotic disorders. Visual task performance and physiological measures of visual processing in relatives may fall on a continuum between typical functioning among

controls and the impairments observed among PwPP (Chkonia et al., 2010; Kéri et al., 2001; Klein et al., 2020b; Pokorny et al., 2021a, 2021b; Schallmo et al., 2013; Schallmo et al., 2015; Sponheim et al., 2006; Yeap et al., 2006). If consistent abnormalities in visual behavior and / or neural processing can be identified across both PwPP and their biological relatives, then such differences may be able to serve as endophenotypes (Calkins et al., 2008; Gottesman and Gould, 2003; Iacono et al., 2017), which could help elucidate the genetic basis of abnormal visual perception in PwPP, for example by aiding the development of animal models.

We chose to take a trans-diagnostic approach to studying visual functioning among PwPP, rather than focusing on specific diagnostic categories (e.g., schizophrenia vs. bipolar disorder). Because the reliability and validity of discrete categories, as defined by the Diagnostic and Statistical Manual of Mental Disorders (DSM), have been criticized (Kotov et al., 2017; Markon et al., 2011), we sought to examine the neurophysiology of visual dysfunction among PwPP more generally, as well as their first-degree biological relatives. Our approach is informed by the National Institute of Mental Health's Research Domain Criteria (RDoC) framework (Cuthbert, 2014), and by the notion that there may be a spectrum of disrupted visual functioning among PwPP and their biological relatives that extends across diagnostic categories and includes genetic liability for psychosis. We hope that our work will help to clarify the etiology of visual dysfunction in psychosis spectrum conditions.

The primary focus of the present study was to examine behavioral and neurophysiological markers of visual functioning in PwPP and their biological relatives. This investigation was carried out using behavioral and 7 T imaging measures as part of the Psychosis Human Connectome Project. These data were collected from the same study population as the 3 T and clinical measures described in our recent publication (Demro et al., 2021). Similar to the original Young Adult HCP (Benson et al., 2018; Glasser et al., 2016; Van Essen et al., 2013; Vu et al., 2017), we collected 7 T fMRI data during a 'sweeping bars' paradigm to facilitate population receptive field (pRF) mapping and functional definition of retinotopic early visual area boundaries. Our pRF paradigm additionally included simultaneous acquisition of auditory and motor responses. We also conducted experiments using visual paradigms focused on aspects of visual perception that may differ among PwPP, as detailed above. Before beginning this study, we solicited input from a small number of experts in the fields of vision science and psychosis research in order to select visual paradigms that might provide valuable and complementary insight into such abnormalities. The paradigms that we selected (in addition to pRF mapping) were contrast surround suppression (CSS), contour object perception (COP), and a bi-stable structure-from-motion (SFM) task (behavioral data only), the details of which are described below (also see Supplemental Information for additional background on the visual tasks that we selected).

This paper describes the motivation, methods, data quality, and general pattern of results (from controls) for each of our 7 T experimental paradigms. Acquiring our fMRI data at 7 T allowed us to achieve higher functional contrast-to-noise and higher spatial resolution versus comparable 3 T methods (Vu et al., 2017), which is advantageous for examining fMRI responses from retinotopically organized visual areas. Further, we conducted 7 T MR

spectroscopy (MRS) experiments to measure neurochemical levels within occipital (OCC) and prefrontal (PFC) cortices, in order to examine hypotheses including whether abnormal neurochemistry contributes to visual dysfunction in psychotic disorders (Foss-Feig et al., 2017; Lisman, 2012). The OCC region was chosen to include areas in early visual cortex that may be relevant to abnormal visual perception in PwPP, whereas the PFC region was selected for its potential role in higher cognitive dysfunction (e.g., decision making, cognitive control) in PwPP (Bonilha et al., 2008; Tully et al., 2014; Venkatraman et al., 2009). Using 7 T MRS provided higher signal-to-noise ratio (SNR) and greater ability to study individual metabolites (e.g., separating glutamate and glutamine, reliably quantifying GABA), in comparison to similar MRS methods at 3 T (Godlewska et al., 2017; Terpstra et al., 2016). However, human brain imaging at 7 T also presents a number of challenges (see Supplemental Information for further details). Repeat scan data from all experiments were acquired from a subset of participants in order to examine longitudinal variability in our behavioral and physiological measures, and any associations with changes in psychiatric symptoms over time. The overall objective of this work is to provide sufficient information about the background, methodology, and data quality to facilitate subsequent investigations using the data, code, and other resources that we have made available as part of the Psychosis Human Connectome Project.

2. Methods

2.1. Participants

Data were collected from three groups of participants: healthy controls with no family history of psychosis (n = 44; controls hereafter), first-degree biological relatives of a person with a history of psychotic psychopathology (n = 46; relatives hereafter), and people with a history of psychotic psychopathology (n = 68; PwPP hereafter). Of these, 1 control, 2 relatives, and 2 PwPP were excluded from our study after completing the experiments described below (e.g., found to have a visual abnormality). Data from excluded individuals are not presented here, unless otherwise noted. Our final sample size was 43 controls, 44 relatives, and 66 PwPP. Demographic and psychiatric symptom data for each group are presented in Table 1. In Supplemental Table 1, data for PwPP are presented within three diagnostic sub-groups (people with schizophrenia, n = 36; those with schizoaffective disorder, n = 10; and those with bipolar I disorder with psychotic features, n = 20). A subset of participants (10 controls, 39 PwPP) returned for a second experimental visit during which repeat scan data were acquired. Because of this, a ‘data set’ in our study refers to data from a single experimental visit and there are more data sets than unique participants.

Inclusion criteria for the Psychosis Human Connectome Project have been described previously (Demro et al., 2021; Schallmo et al., 2021). These criteria included age 18–65 years, English as a primary language, the ability to provide written informed consent, no legal guardian, no diagnosed learning disability or IQ less than 70, no current or past central nervous system disease, no history of head injury with skull fracture or loss of consciousness longer than 30 minutes, no alcohol or drug abuse within the last 2 weeks, or dependence within the last 6 months, no electroconvulsive therapy within the last year, no tardive dyskinesia, no visual or hearing impairment, no condition that would physically

inhibit task performance such as paralysis or severe arthritis. All participants in the PwPP group had a history of schizophrenia, schizoaffective disorder, or bipolar I disorder with psychotic features and were not adopted. Relatives had a biological parent, sibling, or child with a history of one of these disorders (but not necessarily an enrolled participant from the PwPP group) and were not adopted. Relatives included both individuals with and without current psychiatric diagnoses (Table 1). These included individuals with major depressive disorder ($n = 16$) and panic disorder ($n = 2$). Controls had no personal or immediate family history (i.e., parents, siblings, children) of psychosis spectrum disorders. Additional inclusion criteria for 7 T scanning included the ability to fit comfortably within the scanner bore (60 cm diameter) and the radio frequency (RF) head coil (head circumference less than 62 cm), weight less than 440 pounds, and corrected Snellen visual acuity of 20/40 (decimal fraction = 0.5) or better. All participants had completed two 3 T fMRI scanning sessions prior to 7 T scanning. Individuals who exceed a limit of 0.5 mm of head motion per TR (i.e., framewise displacement) in greater than 20% of TRs from all 3 T fMRI runs (approximately 2 h of scanning) were excluded prior to 7 T scanning.

All participants provided written informed consent prior to their participation and were compensated approximately $20 / hour for their time. As part of the informed consent process, participants agreed to have their de-identified data shared publicly, including the dates of all research study visits. All experimental procedures complied with the Declaration of Helsinki and were approved by the University of Minnesota IRB. All participants had sufficient capacity to provide informed consent, as assessed by the University of California Brief Assessment of Capacity to Consent (Jeste et al., 2007).

2.2. Study timeline

The time between 3 and 7 T scanning is shown for each group in Table 1. Typically, the minimum delay was at least 1 week, owing to the need for quality assessment of the 3 T data for screening purposes (as described above, participants with poor 3 T data quality were excluded from 7 T scanning). We conducted repeat 7 T scans for a subset of PwPP and a very limited number of controls (Table 1). This was done in order to permit longitudinal assessment of neural and behavioral measures from the 7 T experiments (i.e., visual behavior, fMRI, MRS), and psychiatric symptom measures acquired on the day of 7 T scanning (i.e., BPRS, SANS, SAPS; see below). The time between the first and second 7 T scans for controls and PwPP is shown in Table 1.

The nomenclature for our different scanning sessions bears explanation. Briefly, we refer to our first iteration of the protocol as 7T-A. Our second protocol iteration, which includes some small changes to the visual stimuli and tasks, is termed 7T-B. Our repeat scans are referred to at 7T-Z. For full details, please see Supplemental Information and Supplemental Table 2.

2.3. Apparatus

Our psychophysical (quantitative behavioral) experiments were conducted in a darkened laboratory on an Apple Mac Pro and an Eizo FlexScan SX2462W monitor with a 60 Hz refresh rate (mean luminance = 61.2 cd/m^2). A Bits# stimulus processor (Cambridge

Research Systems) was also used; when in Mono++ mode, this provided 9.6-bit luminance resolution (for the CSS psychophysical task, see below). Participants were seated in a height-adjustable chair with an adjustable chin rest to maintain a stable head position at a viewing distance of 70 cm. Stimuli were generated and presented using PsychoPy (version 1.85.2; Peirce 2007). Monitor luminance was linearized using a PR655 (Photoresearch, JADAK, North Syracuse, NY) spectrophotometer.

7 T MR data were acquired on a Siemens MAGNETOM scanner. This scanner was equipped with an 8-kW RF power amplifier and body gradients with 70 mT/m maximum amplitude and 200 T/m/s maximum slew rate. The scanner software was upgraded from VB17 to VE12U in July 2019. Data quality before and after the upgrade was comparably high (e.g., temporal SNR, image SNR; data not shown). For both MRS and fMRI, participants were given head, neck, and lumbar padding, and instructed to minimize movement during scanning. For our MRS data acquisition, we used a custom-built RF head coil with two surface ^{1}H quadrature transceivers, one for the front of the brain and one for the back of the brain. Participants were removed from the scanner in between occipital and prefrontal MRS scans (during the same scanning session), in order to switch the coil configuration. A 7 T MR-compatible motion tracking system (Metria Innovation Inc., Milwaukee, WI) was used to track a Moiré Phase Tracking marker attached to the participant's face in order to measure head motion during MRS (but not during fMRI). Head motion was observed by an experimenter in real time. When head motion > 5 mm was observed, MRS scans were repeated, and participants were encouraged to remain still. Participants were removed from the scanner in between MRS and fMRI data acquisition, in order to change scanning equipment. For fMRI data acquisition, we used a Nova Medical (Wilmington, MA) RF head coil (1 transmit and 32 receive channels). We used 5 mm thick dielectric pads (3:1 calcium titanate powder in water) positioned under the neck and beside the temples during the fMRI experiments, when possible (allowing for the participant's comfort). Previous 7 T MRI studies as part of the HCP have shown this improves transmit B_1 homogeneity in the cerebellum and temporal lobe regions (Vu et al., 2015).

During fMRI scanning, visual stimuli were presented using an NEC projector with a 60 Hz refresh rate (mean luminance = 271 cd/m^2). Participants viewed stimuli projected onto a 3M (Maplewood, MN) Vikuiti acrylic screen at the back of the bore through a mirror mounted to the head coil, with a viewing distance of 100 cm. Participants used a Current Designs (Philadelphia, PA) MR-compatible 4-button response box during the visual tasks. Auditory stimuli were delivered through Sensimetrics (Gloucester, MA) earbuds, placed in the participant's auditory canals by research staff and covered by medical tape, to minimize the possibility that the earbuds became dislodged while the participant was getting into position in the scanner. We confirmed that participants could hear auditory stimuli presented through the stimuli prior to scanning.

2.4. Experimental protocol

2.4.1. Clinical measures—Details regarding our clinical data collection methods are provided in the Supplemental Information.

2.4.2. Tasks

Population receptive field (pRF).: Each participant completed at least one population receptive field (pRF) mapping scan (Dumoulin and Wandell, 2008) for the purpose of retinotopic mapping in visual areas, as well as simultaneous mapping of auditory and motor regions (see below). During the task, participants were asked to maintain fixation on a central point while a bar moved across the visual field at one of eight orientations (West (W) – East (E), North (N) - South (S), NW - SE, NE - SW, E - W, SE - NW, S - N, SW - NE; Fig. 1A). The moving bar was populated with dynamic and highly salient visual stimuli from Kriegeskorte et al. (2008). The 96 images were divided into 7 categories: human face, human body, animal face, whole animal, food, manipulable objects, and places. An 8th category, noise, was created by Fourier phase-scrambling the three color channels of each image and re-combining the channels to make brightly colored textures with spatial frequencies similar to the object images. Each category was presented during two bar sweeps, chosen randomly. Reduced-contrast noise images were present as a background during all image categories to ensure coverage of the entire bar while minimizing crowding between object images. The bars flickered at either 2 or 12 Hz. The length of the bars spanned a 16° disk and subtended 2° of visual angle in width and traveled across the visual field out to 8° eccentricity. Each bar took 16 s to complete the movement across the visual field, and each bar sweep direction occurred twice in a single scan, once with a 2 Hz refresh rate and once at 12 Hz. There were 4 s of rest between each bar sweep and 4 s of rest at the beginning and end of each scan, such that each scan took 324 s.

During the scan, participants heard auditory tones that varied in pitch (13 tones between 250 and 4000 Hz; Fig. 1B) for the purpose of tonotopic mapping (Allen et al., 2022; Da Costa et al., 2011; Moerel et al., 2014; Norman-Haignere et al., 2013). Auditory tones were presented through the headphones in the presence of constant scanner sounds (i.e., no ‘gap’ in the scanning sequence). In an auditory block, each of the 13 tones were presented in either ascending (i.e., 250–4000 Hz) or descending (i.e., 4000–250 Hz) order for 500 ms with a 500 ms inter-stimulus intervals. Because our fMRI scanning sequence had a 1 s TR, the scanner sounds from each TR occurred at a fixed time relative to the tone presentation. A full auditory block was 13 s long. For each run of the pRF task, there were 8 auditory blocks in the first half of the scan (ascending tone order in run 1, descending in run 2) followed by 8 auditory blocks in the second half of the scan (descending in run 1, ascending in run 2). There was a 10 s silent period (scanner noise only) at the beginning and end of each run, and 96 s in between the ascending and descending tone sets.

Participants were asked to complete a motor tapping task during the pRF paradigm, to facilitate functional mapping of motor cortex (Lotze et al., 2000; Olman et al., 2012). In this task, they were asked to press the left or right buttons on the button box, curl the toes on their left or right feet, and tap their tongue to the roof of their mouth in time with the presentation of a flashing body part cue image presented at fixation (Fig. 1C). Motor cues were presented for 500 ms followed by a 500 ms presentation of a fixation cross, with a motor block duration of 13 s. It was not an intentional aspect of the design that both the motor blocks and the auditory sweeps lasted 13 s. Originally, 12 tones were included in the auditory design; the sweeps were not intended to cycle at the same frequency as the motor

task. In the process of optimizing the auditory stimulus, a 13 th tone was generated and the fact that this created cycles with the same duration as blocks in the motor condition was unfortunately overlooked.

For most participants, two 324 s pRF mapping runs were completed. Because adequate maps may be extracted from the data from a single run, the second scan was omitted from the end of a scanning session if the participant was experiencing fatigue or discomfort (3 of 52 scanning sessions for controls had only one pRF scan, 10 of 40 for relatives, and 38 of 84 for PwPP).

Participants viewed the task before entering the scanner, to practice tapping in response to the motor cues. Once participants were settled in the scanner, a sound check was performed. The sound check consisted of playing the tones that would occur during the pRF task while an EPI scan was being acquired. After that scan participants were asked to indicate whether they could hear the tones over the noise of the scanner.

Example pRF results from individuals and a group of control participants are shown in the Results section. As this manuscript focuses on describing data acquisition methods and data quality, details of the data processing and analysis for the pRF experiment are relegated to the Supplemental Information.

Contrast surround suppression (CSS) task.: For the CSS task, participants were asked to determine which of two briefly presented sinusoidal luminance gratings—presented to the left or right of a fixation mark—had higher contrast. Examples of the CSS stimuli are shown in Fig. 2A.

In the psychophysical experiment, gratings were presented on a mean gray background at seven pedestal contrast levels: 0, 0.65, 1.25, 5, 10, 20%. The range of pedestals was chosen based on previous studies (Boynton et al., 1999; Legge and Foley, 1980; Schallmo et al., 2016; Yu et al., 2003; Zenger-Landolt and Heeger, 2003) to allow investigation of threshold and suprathreshold contrast discrimination. Two gratings (2° diameter) were presented, each at 3° eccentricity to the left and right of a central fixation point (0.2° square; white with black outline) along the horizontal meridian. Gratings were contrast reversing at 4 Hz, and had a spatial frequency of 1.1 cycles/°. Four target orientations were used: vertical, horizontal, and diagonal ± 45°. In some trials, the 10% contrast pedestal was presented with a surrounding sinusoidal grating annulus with inner and outer diameters of 2.5° and 4°, respectively (contrast = 100%; parallel to the target grating). The edges of the target and surrounding stimuli were blurred with a raised cosine function. A small fiducial circle (2.1° diameter with 0.05° gap between target grating and circle line; dark gray, luminance = 31.1 cd/m^2) outside the target location was used to reduce spatial uncertainty about the target position. On each trial, a contrast increment was added to one of the two target gratings. The contrast increment was adjusted across trials within a range of 0.13–40%, according to a Psi adaptive staircase method (Kingdom and Prins, 2010) implemented in PsychoPy, to find the minimum contrast increment that could be perceived with 80% accuracy (i.e., contrast discrimination threshold for that pedestal contrast). For twelve early participants (part of the 7T-A protocol), we ran a pilot version of the task with slight differences (see Supplemental

Information for more details about task differences; for the number of data sets collected for each version of the task, see Supplemental Table 2). Pilot task data are not included in the results presented below.

Participants were instructed to maintain fixation at the center of the screen while using their peripheral vision to determine which target grating was higher contrast. CSS task timing is illustrated in Fig. 2B. Each trial began with an audio tone (250 ms) and presentation of the central fixation square and the two target gratings for 800 ms. Participants indicated their response on a keyboard using the left or right arrow key. The response period was not limited in duration, with a minimum inter-trial interval of 400 ms. The task was divided into eight blocks, one per pedestal contrast condition plus one block with the 10% pedestal plus the surrounding annulus. Each block included 90 trials from three separate interleaved staircases (30 trials / staircase), which yielded 3 independent threshold estimates per condition. Each block also contained 20 catch trials (not included in the staircases), in which the contrast increment was set to the maximum value (45%), in order to assess off-task performance. Each block lasted approximately 4 min, with self-timed rests between blocks. Participants were also instructed that they could take a brief pause within a block by withholding their response to the current trial. Task instructions and practice example trials were presented at the beginning of the psychophysical experiment. Total task duration (including instructions and practice) was approximately 40 min.

In the fMRI experiment, gratings were presented at five pedestal contrast levels: 0, 10, 20, 40, 80%. This range of pedestals was chosen based on previous fMRI studies (Zenger-Landolt and Heeger, 2003). Gratings were presented with the same size, positions, and spatial frequency as in psychophysical experiments. Grating orientation was randomized across stimulus presentations in a range of 0°−180° in 15° increments. For each of the five pedestal contrasts, target gratings were presented either with or without a surrounding sinusoidal grating annulus with inner and outer diameters of 1.25° and 2°, respectively (100% contrast; same orientation as center).

CSS fMRI task timing is shown in Fig. 2C. Each trial began with the presentation of the stimuli for 750 ms followed by a blank screen with a central fixation square presented for 1.05 s (600 ms response window after stimulus offset, 450 ms inter-trial interval, 1.8 s total trial-to-trial onset). Trials were presented within blocks of 5 trials (9 s per block). Within each block, the target contrast pedestal was either 0, 10, 20, 40, or 80% for all 5 trials. Ten blocks (5 ‘target on’ with pedestal contrast at either 0, 10, 20, 40, or 80%, 5 ‘target off’ with pedestal contrast at 0%) composed each condition. Within each condition, ‘target on’ and ‘target off’ blocks were presented in an alternating order, starting with a ‘target on’ block and ending with a ‘target off.’ This yielded an on-off block presentation order with 5 cycles per 90 s condition. Target pedestal contrast (10–80%) and surround contrast (0 or 100%) were held constant within each condition, for a total of 8 stimulus conditions in the main experiment. The experiment was divided into 3 fMRI runs, each 5 min long, with 3 conditions presented in each run. Each condition was presented only once across all runs, and the order of the 8 conditions in the main experiment was randomized across participants to one of 4 possible pseudo-random presentation sequences.

The first condition in the first fMRI run was always a functional localizer condition (also 90 s long, also divided into 10 blocks of 9 s each), which was designed to define regions within primary visual cortex representing the target stimuli. Here, we used a differential localizer technique (Olman et al., 2007), in which blocks of target gratings without surrounds (pedestal contrast = 80%, surround contrast = 0%) alternated with surround-only blocks (target pedestal contrast = 0%, surround contrast = 100%). This allowed us to isolate voxels in retinotopic early visual areas that responded more strongly to target stimuli than to surrounding gratings, as in previous work (Qiu et al., 2016; Schallmo et al., 2016, 2018, 2020). This first functional localizer condition was contiguous with the rest of the first CSS functional run (i.e., not a separate fMRI run).

In all of the CSS fMRI conditions, contrast increments were added to one of the two target gratings on each trial, as in our psychophysical experiment. This was done to equate task difficulty across conditions, and to keep the participants engaged and attending to the target stimuli. On each trial, participants indicated on which side the increment appeared using the left- or right-most button on a 4-button response box (Current Designs, Philadelphia, PA). The fixation square turned green upon correct responses. The response period (during the blank after each stimulus presentation) timed out after 600 ms. During our fMRI task, contrast increments were controlled by a 3-down, 1-up staircase using PsychoPy, with separate staircases for each of the 10 target pedestal (0, 10, 20, 40, or 80%) and surround (0 or 100%) combinations. There were 30 ‘target on’ and 30 ‘target off’ trials (on separate staircases) within each condition. The minimum contrast increment was 1%, and maximum contrast increment within each staircase was 25% of the target pedestal contrast, or 3% contrast, whichever was greater. At the beginning of the fMRI experiment, participants were briefly reminded of the task instructions, and were told that the task would not wait for them to respond, unlike during psychophysics.

Example CSS results from individuals and a group of controls are shown in the Results. Full details of the CSS data processing and analysis are provided in the Supplemental Information.

Contour object perception (COP) task.: Visual stimuli in the COP experiment (Fig. 3A-D) were based on those previously used by Silverstein and others (Silverstein et al., 2009, 2006, 2015, 2000). Stimuli consisted of a grid of 170 Gabor line elements, 14° visual angle wide by 11.3° tall. Gabor elements had a Gaussian envelope with $SD = 0.067°$ and a spatial frequency of 5 cycles/°, with 2 cycles visible within each ~0.4° wide (6 *SD*) Gabor. Of the 170 Gabor elements, 155 comprised the background, with a minimum spacing of 0.8° visual angle. The remaining 15 elements positioned around the center of the display formed an egg-shaped contour object that either pointed towards the left or right. This egg contour was 5.9° wide by 4.7° tall. Gabor elements that composed the egg were positioned with a minimum spacing of 1.09° and a maximum spacing of 1.13° relative to one another along the contour axis. One thousand exemplar stimulus grids were procedurally generated and saved for presentation during the task (chosen randomly). To manipulate the detectability of the contour stimuli, the relative orientation of each Gabor element within the contour was jittered with respect to the axis of the egg. This was done in steps of ± 3° between 0° (perfectly aligned) and 45° (completely scrambled). SNR, defined as the average spacing

between adjacent background elements divided by the average spacing between adjacent contour object elements, was 0.87.

In our COP psychophysical experiment, three different types of trials were presented with different stimuli: scrambled (45° jitter) contour stimuli presented without background elements (i.e., catch trials, used to assess off-task performance), aligned (0° jitter) contour stimuli presented within a field of background elements (to measure discrimination accuracy for fully aligned contours), and jittered contour stimuli presented with background elements. In this third condition, the alignment of the Gabor elements was manipulated across trials to identify the specific degree of orientation, or jitter threshold, at which the participant would discriminate directionality of the egg (left or right) with 70% accuracy. Contour jitter varied in increments of 3° from 0° to 45°. Contour jitter varied across trials based on a Psi adaptive staircase method (Kingdom and Prins, 2010), implemented within PsychoPy.

The COP psychophysical task was divided into two blocks, with each block consisting of three independent interleaved staircases of 30 trials of the jittered contour stimuli. Each block also included 20 additional trials of the scrambled contour stimuli with no background, and 20 of the aligned contour stimuli with a background. The experiment began with instructions asking participants to fixate on a square at the center of the screen and use their peripheral vision to decide whether the egg-shaped contour object was pointing towards the left or the right. They were told to make their best guess if they were unsure in which direction the egg was pointing. Blocks began with a central fixation square presented for 1500 ms, followed by presentation of the stimulus for 1000 ms, and an unlimited response period during which participants used the left and right arrow keys on a keyboard to provide an answer (Fig. 3E). The order of trials was randomized within each block, and participants were allowed to take a self-timed rest between blocks. They were also told that they could take a short pause during the block if needed by withholding their response until they were ready to proceed. Each block lasted about five minutes, with a total task duration including instructions of approximately 15 min.

The fMRI version of the COP task was analogous to that used in our psychophysics experiment, with a few differences (Fig. 3E). Four types of stimuli were presented, and these were divided into different conditions: jittered or fully scrambled contours, presented either with or without background elements. Scrambled contours with backgrounds were included in the fMRI task in order to measure responses to a field of Gabors in which the contour was very difficult (if not impossible) to perceive. For the jittered with background condition, contour stimuli were presented with their degree of orientation jitter controlled by a 3-up, 1-down adaptive staircase. Jitter level began at 0° at the start of the fMRI task run, and changed in increments of ± 3°. These staircases are expected to converge at the jitter level for which a participant could detect the directionality of the egg with 79% accuracy (Garcia-Perez, 1998). Contour jitter in the jittered without background condition was matched to the jittered with background condition across blocks. The contour stimuli in the scrambled conditions were completely scrambled (45° of jitter). Stimuli were presented in trials with a 1 s stimulus duration, followed by a randomized inter-stimulus interval of 2–4 s. In between each trial, a white fixation square was presented on a mean gray background with no background Gabors present. Trials were organized into two types of blocks (24 s

long): those with and those without background elements. Each block included six trials; four jittered and two scrambled trials per block. The experiment began with a block of stimuli with background elements, and alternated between the two block types. Six blocks were administered per fMRI run. There was an additional 12 s of rest before and after the 6 main experiment blocks in each run. A single fMRI task run lasted 6 or 9 min in total (see below), and each participant completed 2 fMRI runs within a single scanning session.

The instructions provided to the participant during the COP fMRI task were identical to those given during the psychophysics experiment, with the exception of being asked to provide a response as soon as possible after stimulus presentation.

The COP fMRI paradigm also included a functional localizer condition. Data from the functional localizer condition were acquired to permit identification of retinotopic regions of visual cortex that represented the spatial position of the egg stimuli. This condition consisted of repeated presentations of egg-shaped contours of Gabor elements, without background elements. In order to facilitate strong fMRI responses in early visual cortex, Gabor elements reversed contrast at a frequency of 2 Hz. Alternating blocks of rest (fixation only) and localizer stimuli were administered, each lasting 12 s. During the localizer stimulus blocks, the contrast reversing egg randomly changed directionality (left or right) every 2 s. Seven blocks of rest and 6 blocks of localizer stimuli were presented during the functional localizer condition, which lasted about three minutes. The functional localizer condition was presented at the beginning of the first COP fMRI run, prior to the first main experimental block, which meant that this first COP run was longer than the second (9 min in total, rather than 6). We note that while the functional localizer for the COP task was designed to identify voxels that responded more strongly to contour vs. rest (i.e., fixation only), it was not designed to localize voxels that responded more to the contour vs. the background. Thus, some voxels within our COP ROIs responded to both contour and background stimuli, which led to the increase in the fMRI response for the background vs. no background conditions in the COP task (see Fig. 9).

Both the psychophysical and fMRI paradigms for the COP task were modified slightly after an initial piloting phase (about 6 months after the study's onset, when the change from protocol version 7T-A to 7T-B was made). This was done to make the task easier, especially for PwPP, by making the spacing between background and contour Gabor elements wider (SNR was increased from 0.75 to 0.87), thereby making the contour elements easier to perceive. For full details, please see the Supplemental Methods, and Supplemental Table 2.

Example COP results from individuals and a group of control participants are shown in the Results. Full details of the data processing and analysis for the COP experiment are included in the Supplemental Information.

Structure-from-motion (SFM) task.: We collected psychophysical behavioral data during a SFM task using the rotating cylinder illusion; SFM fMRI data were not acquired, due to time constraints. The visual stimuli in our SFM psychophysical task (Fig. 4A) were standard rotating cylinders (Treue et al., 1991; Ullman, 1979). The rotating cylinder is a classic illusion in which small visual elements (here, black and white squares) move back and

forth across a rectangular area in order to induce the perception of a 3-dimensional cylinder rotating in the depth plane. The rotating cylinder stimuli used here were composed of 400 small black and white squares (each 0.25° wide; 200 black and 200 white) that alternated between moving from the left to right and right to left across the width of a rectangular area, and each positioned pseudo-randomly along the height of the rectangular region (height = 10°, width = 7°). The squares sped up as they approached the center of the rectangle and slowed down as they approached each edge. This was done to simulate the perceived speed of the squares as if they were positioned on a transparent cylinder rotating in the depth plane (simulated rotation speed of 90°/s).

Two versions of the stimuli with subtle but important differences were used for the two different task conditions, referred to as the bi-stable and real switch tasks. In both tasks the same black and white squares moved back and forth across the rectangular area with speed, size, and position being constant across the two tasks. In the bi-stable task, a small red fixation point (0.6° diameter) was positioned in front of all squares in the center of the rectangular area (Fig. 4A). When dots collided in the bi-stable task, they occluded one another randomly, to remove this potential depth cue. In the absence of inherent depth cues, the direction of motion is ambiguous, and perception spontaneously alternates between the front surface rotating to the left and to the right. In the real switch task, we simulated physical switches of the rotation direction in depth by changing which set of dots (i.e., those rotating left to right or right to left; surface #1 and surface #2 of the cylinder) were presented in the front or back. To do so, we used the same red fixation dot overlaid on another larger blue circle (1.8° diameter) and alternated which set of dots passed in front of or behind each other and the larger fixation circle (Fig. 4B). This provided an explicit depth cue thus biasing one percept (e.g., front rotating to the left) to become dominant. Switches occurred every 9–13 s (order and timing were pseudo-randomized, but fixed and identical for all participants). The real switch task was added to the experiment during the 7T-A data collection phase, about 2 months before the switch to the final 7T-B protocol. This permitted us to assess participants' ability to perceive and respond to real switches in rotation direction. Thus, data are missing from a number of the early participants (7T-A) who did not complete this condition.

In both SFM task conditions, participants were asked to fixate on the small central red circle and told to use their peripheral vision to determine the direction of rotation of the front surface of the cylinder, either left or right (Fig. 4C). Participants were instructed to respond using the left or right arrow keys to indicate which direction of rotation they perceived. Importantly, they were told to respond immediately to their initial percept at the beginning of the stimulus presentation, and then again each time their perception changed. Each participant first completed a short (30 s) practice version of the real switch task. Participants then ran one block of the real switch task followed by 5 blocks of the bi-stable task. Each block was 2 min long; the rotating cylinder was presented for the entirety of the block.

Example SFM results from individuals and a group of control participants are shown in the Results. Additional details of the SFM analysis are included in the Supplemental Information.

Eye tracking.: Eye tracking data were acquired during our psychophysical experiments using an SR Research (Ottawa, Canada) Eyelink 1000 infrared eye tracker (1000 Hz sampling rate, binocular acquisition). The camera was mounted on the table in front of the participant, below the monitor. Nine point calibration and validation were performed prior to each psychophysical task, and drift correction was performed in between task blocks.

During fMRI, eye tracking data were acquired from a subset of participants using either an SR Research Eyelink 1000 (mounted at the back of the scanner bore), or an Avotec (Stuart, FL) Nano infrared eye tracker (mounted inside the Nova RF head coil). Information on the number of eye tracking data sets collected in each task across participant groups is presented in Supplemental Table 4. Note that due to logistical and safety issues during the COVID-19 pandemic, eye tracking data were not collected during fMRI experiments between March, 2020 and July, 2021.

Functional magnetic resonance imaging (fMRI).: FMRI data acquisition parameters followed the 7 T scanning protocol in the original Young Adult HCP (Glasser et al., 2016; Van Essen et al., 2013; Vu et al., 2017, 2015), as described below. Full details of our scanning protocols are included in the Supplemental Materials. Gradient echo (GE) fMRI data were acquired with TR = 1000 ms, TE = 22.2 ms, echo spacing = 0.64 ms, flip angle = 45°, resolution = 1.6 mm isotropic, partial Fourier = 7/8, 85 oblique-axial slices, field of view = 208 × 208 mm^2, phase encode (PE) direction = anterior-posterior, multi-band acceleration factor = 5, parallel imaging acceleration factor = 2. A single GE scan (3 TRs) was acquired with identical parameters as above, but with an opposite PE direction (posterior-anterior), to facilitate geometric distortion compensation (Schallmo et al., 2021). A T_1-weighted structural scan was acquired with TR = 3000 ms, TE = 3.27 ms, echo spacing = 8.1 ms, flip angle = 5°, resolution = 1 mm isotropic, partial Fourier = 6/8, 176 oblique-axial slices, field of view = 256 × 256 mm^2 , parallel imaging acceleration factor = 2. A B_0 field map was acquired with TR = 642 ms, TEs = 4.08 & 5.1 ms, flip angle = 32°, resolution = 1.6 mm isotropic, partial Fourier = 6/8, 85 oblique-axial slices, and field of view = 208 × 208 mm^2. A pair of spin echo (SE) scans (3 TRs each) with opposite PE directions (anterior-posterior and posterior-anterior) were acquired with TR = 3000 ms, TE = 60 ms, echo spacing = 0.64 ms, flip angles = 90° & 180°, resolution = 1.6 mm isotropic, partial Fourier = 7/8, 85 oblique-axial slices, field of view = 208 × 208 mm^2, multi-band acceleration factor = 5, parallel imaging acceleration factor = 2. The imaging field-of-view positioning (yellow box in Fig. 5A) was standardized using Siemens AutoAlign. An example sagittal image from a GE EPI scan in a single participant is shown in Fig. 5B.

In order to reduce magnetic field inhomogeneity, B_0 shimming was performed within a 130 × 170 × 120 mm^3 oblique-axial region (i.e., adjustment volume; green box in Fig. 5A), centered on the brain. We measured the linewidth of water in the Siemens Interactive Shim tab; for values > 80 Hz, shim currents were re-calculated to obtain a better shim solution. We used a local software program (*shimcache*) to apply the computed shim values before each scan to ensure there was no loss of B_0 shim values during scanning.

Magnetic resonance spectroscopy (MRS).: MRS offers a non-invasive method for examining several metabolites of interest in psychosis. As noted in the Introduction, examining glutamate and GABA concentrations may be relevant for understanding neural dysfunction among PwPP. However, it is also worth noting that these MRS markers do not directly reflect neural excitation or inhibition *per se*. Glutamate and GABA are found at much higher concentrations within presynaptic neurons than in the synaptic cleft; experimental evidence suggests that GABA concentrations are about 1 mM intracellularly, and glutamate is found at intracellular concentrations of about 5–10 mM, whereas extracellular concentrations of glutamate and GABA have been reported in the low micromolar range (about 2 μM; Cavelier et al., 2005; Featherstone, 2010; Wu et al., 2007). Only a portion of the intracellular glutamate and GABA in the brain is localized in presynaptic terminals, and there are also substantial metabolic pools within cell bodies (Rae, 2014). Thus, it can be difficult to draw strong conclusions about the role of these metabolites as neurotransmitters (versus other metabolic functions) from MRS data alone. Glutamine is another important player in the glutamate and GABA metabolic cycles that may be relevant for understanding abnormal neurochemical functioning among PwPP. After glutamate is released from pre-synaptic neurons, it is taken up by astrocytes, converted to glutamine, transported back to pre-synaptic neurons, and converted back to glutamate (Schousboe and Sonnewald, 2016). In addition, glutathione plays a number of important roles in brain function, including as an anti-oxidant, and glutathione functioning may also be disrupted among PwPP (Matsuzawa et al., 2008; Perkins et al., 2020).

Occipital cortex (OCC).: For our MRS experiments in OCC, we acquired data using a stimulated echo acquisition mode (STEAM) sequence (Marjańska et al., 2017) with the following parameters: TR = 5000 ms, TE = 8 ms, mixing time (TM) = 32 ms, hsinc pulse = 1.28 ms, volume-of-interest (VOI) size = 30 mm (left-right) x 18 mm (anterior-posterior) x 18 mm (inferior-superior), transmitter frequency = 3 ppm, 3D outer volume suppression interleaved with variable power and optimized relaxation delay (VAPOR) water suppression (Tkáč et al., 2001). Chemical shift displacement error was 4% per ppm. We acquired 2048 complex data points with a 6000 Hz spectral bandwidth. The OCC VOI was placed within the medial occipital lobe, superior to the cerebellar tentorium, posterior to the occipitoparietal junction, and anterior to the sagittal sinus (Fig. 5C and D). This mid-occipital VOI encompasses early visual cortical areas including V1, which are involved in visual functions including perception of motion and contrast, spatial context processing, and contour integration. We chose to keep this VOI aligned squarely within the occipital lobe (based on Siemens AutoAlign), in order to: (1) position the VOI within the region of maximal transmit signal based on the geometry of our occipital surface coil, and (2) maximize positioning consistency across scanner operators. For repeat (7T-Z) scans, VOIs were placed in the same anatomical position as in the first scan using a saved copy of the scan protocol along with AutoAlign. The full details of our scanning protocols are included in the Supplemental Materials. We note that our study conforms to the minimum reporting standards for MRS work recently recommended by a group of MRS experts (Lin et al., 2021).

Our acquisition protocol was as follows. We began by acquiring a T_1-weighted anatomical scan to facilitate voxel placement, using the following parameters: TR = 2500 ms, TE = 3.2 ms, echo spacing = 7.9 ms, flip angle = 5°, resolution = 1.3 mm isotropic, partial Fourier = 6/8, 64 mid-sagittal slices, field of view = 160 × 160 mm^2 . After positioning the OCC voxel based on the individual participant's occipital anatomy, we performed shimming within the VOI using FAST(EST)MAP (Gruetter, 1993; Gruetter and Tkáč, 2000) to obtain a linewidth of water ≤ 15 Hz (measured using Spectroscopy card in Siemens software), repositioning the voxel slightly as necessary. The B_1 field for the 90° pulse and the water suppression flip angles were calibrated by adjusting the transmit voltage for each VOI in each participant. We then conducted a brief STEAM scan (4 TRs) to review the quality of water suppression. Next, we acquired our primary metabolite STEAM spectra (96 shots or TRs; 8 min), from which metabolite concentrations were quantified. Finally, three additional reference scans were acquired without water suppression to permit eddy current correction and absolute quantification of metabolite concentrations relative to water. The first was the same as the previous STEAM scan, but with the transmitter frequency = 4.7 ppm, and without VAPOR water suppression (1 TR). The second was the same as the first, but included 4 TRs to permit phase cycling. The third was the same as the first (1 TR), but did not include outer volume suppression.

Prefrontal cortex (PFC).: We acquired STEAM data within PFC using the same protocol as for OCC, except that the VOI size = 30 mm (left-right) by 30 mm (anterior-posterior) by 15 mm (inferior-superior). The PFC voxel was oriented obliquely within the sagittal plane, and placed within the dorsomedial prefrontal cortex, dorsal and anterior to the cingulate gyrus, along a line extending 135° from the anterior edge of the genu of the corpus callosum (Fig. 5E & F). This region was chosen based on our review of previous prefrontal MRS studies among PwPP (Egerton et al., 2017; Öngür et al., 2010b; Rowland et al., 2013; Salavati et al., 2014; Wijtenburg et al., 2015). Although some previous MRS studies have used VOIs that included portions of both the dorsomedial prefrontal cortex and the anterior cingulate cortex, we chose to avoid including the anterior cingulate in this study, in an attempt to limit the functional heterogeneity of the tissue within our VOI. We also sought to place the VOI within the region of maximal transmit efficiency based on the geometry of our prefrontal surface coil, and to facilitate inter-operator consistency. The dorsomedial prefrontal cortex is thought to be involved in a number of cognitive functions affected by schizophrenia, including cognitive control and decision making (Bonilha et al., 2008; Tully et al., 2014; Venkatraman et al., 2009). Our PFC and OCC VOIs were intended to complement one another (e.g., to permit testing the specificity of possible associations between MRS data from a given VOI and visual task measures). PFC data acquisition did not begin until January, 2018, when the frontal MRS coil became available; MRS data sets acquired prior to this included OCC data only. For an initial group of 30 participants with PFC data, we acquired 128 shots (TRs) of metabolite STEAM data. After ensuring that data quality was comparable between PFC and OCC, we reduced this number to 96 shots for subsequent participants, in order to shorten the scan time and reduce participant burden. OCC data were always acquired prior to PFC data within a scanning session. Participants were removed from the scanner in between OCC and PFC scans, in order to switch from posterior to anterior transceiver coils. The entire MRS experiment duration was

approximately 80 min (40 min each for OCC and PFC). MRS data were always acquired prior to fMRI scanning. Participants were removed from the scanner between MRS and fMRI scans and given a short (~30 min) break, during which we prepared the scanner environment for the fMRI experiments.

2.5. Data processing

We provide a summary of fMRI and MRS data processing pipelines in the Supplemental Information. This processing enabled us to assess data quality and the general pattern of results, as presented in the Results section.

2.6. Data quality assessment

2.6.1. Psychophysical & fMRI data quality—We assessed multiple retrospective quality metrics for the psychophysical and fMRI data from our visual tasks. For the CSS and COP psychophysical tasks, poor task engagement was defined as achieving less than 80% (CSS) or 85% accuracy (COP) across all catch trials. For the SFM psychophysical experiment, poor task engagement was defined based on performance in the real switch task as having fewer than 7 correct responses (< 63.6% accuracy) made within 4 seconds of a physical stimulus change.

For fMRI data quality, we first defined excessive head motion during a given task as having ≥ 0.5 mm of motion (i.e., framewise displacement) across > 20% of TR pairs. This was quantified using AFNI's *gen_ss_review_scripts.py*, based on the Euclidean norm of the six head motion parameters from AFNI's *3dvolreg*. We also quantified the fraction of stimulus presentations in each fMRI task for which a behavioral response was recorded (either correct or incorrect, assuming a response was required), as a measure of task engagement. For the pRF fMRI task, we defined poor task engagement as having made no button press responses (at all) during > 10% of left- and right-hand finger tapping blocks in the motor tapping task. During the CSS and the COP fMRI tasks, we defined poor task engagement as not responding to > 10% of all stimulus presentations.

2.6.2. MRS data quality—We examined a number of metrics to assess the quality of our MRS data. First, we measured the linewidth of the unsuppressed water signal (in Hz), which provides a measure of the shim quality (i.e., B_0 homogeneity) within the selected VOI. Poorer shim quality will reduce the fidelity with which different peaks can be resolved in the spectrum. Specifically, we quantified the linewidth of the unsuppressed water signal (FWHM in Hz) within the MRS VOI during the scanning session by fitting a mixed Gaussian-Lorentzian function in the Spectroscopy tab on the Siemens console, as described above, to a phased water signal. This linewidth value was assessed prospectively (i.e., prior to MRS data acquisition), and manually recorded by the scanner operators. We set an *a priori* threshold for poor shim quality as a water linewidth of > 15 Hz. When linewidth values exceeded this limit, shimming was performed again to obtain a better shim solution. Head motion during MRS data acquisition was also examined prospectively using a Metria motion tracking system, as noted above. A very small minority of MRS data sets ($n = 3$) were acquired with shim values > 15 Hz (e.g., cases in which better shim solutions could not be found). Additionally, the spectrum linewidth and SNR as quantified using LCModel

were also used as retrospective MRS data quality metrics. LCModel defines SNR as the maximum signal (*N*-acetylaspartate peak) minus baseline divided by twice the root mean square of the residuals. We set data quality thresholds for these two metrics based on *post hoc* inspection of the data. Poor data quality was defined as > 5 Hz spectrum linewidth, or SNR < 40.

Our MRS data quality allowed us to quantify concentrations for 18 metabolites (for the full list of quantified metabolites, please refer to the Supplemental Information) including the excitatory and inhibitory neurotransmitters glutamate and GABA (respectively).

2.7. Data analysis

For this report, we preprocessed all datasets to compute data quality metrics and compare across groups. We present behavioral, fMRI, and spectroscopy results for controls in order to show representative results, rather than an exhaustive analysis. Analyses were performed in MATLAB (version 2016a) unless otherwise noted. Details of our analysis methods are provided in the Supplemental Information.

2.8. Statistics

We performed statistical analyses of group differences between controls, relatives, and PwPP in terms of demographic, cognitive, and symptom measures (Table 1), psychophysical and fMRI data quality metrics (Supplemental Table 5), and MRS data quality metrics (Supplemental Table 6). We used repeated measures ANOVAs (*F*-values) in cases where data were normally distributed with equal variance across groups (based on visual inspection). Otherwise, we used Kruskal-Wallis nonparametric 1-way ANOVAs (X^2-values), in which cases we excluded repeat scan data, as Kruskal-Wallis tests cannot acommodate repeated measures. For our assessment of clinical measures over time (Supplemental Fig. 2), we calculated Pearson correlations (*r*-values) and intra-class correlations (ICC(3,k); Koo and Li 2016) to quantify longitudinal variability, as well as paired *t*-tests to quantify changes across sessions (Supplemental Table 3).

2.9. Code and data availability

Our experimental task code and our data processing code are available from GitHub (github.com/mpschallmo/PsychosisHCP). Unprocessed (i.e., DICOM) imaging data and associated behavioral data files will be available from the Human Connectome Project (db.humanconnectome.org; data release planned in 2023). Note that the publicly available data from each scanning session are in native (i.e., scanner) space. Details of our procedures for integrating data across scanning sessions are provided in the Supplemental Information. Clinical and other (non-imaging associated) behavioral data, as well as notes for each scanning session, will be available from the National Data Archive (nda.nih.gov/edit_collection.html?id=3162). Processed data will be made available by the investigators upon request.

3. Results

In order to characterize visual perceptual functioning in PwPP, we acquired neurophysiological data from a group of 43 healthy controls, 44 biological relatives, and 66 PwPP. The dataset includes visual psychophysical (i.e., behavioral task) data and 7 T functional MRI data, using tasks focused on basic aspects of visual perception (e.g., retinotopy, context processing, object perception). We also acquired 7 T MR spectroscopy data in the occipital and frontal lobes, in order to characterize the concentrations of different metabolites in these same participants. A subset of PwPP and controls were recruited to return for an identical repeat session a few months after their initial experimental session (see Table 1 for information about the time between first and repeat sessions). Table 2 summarizes the number of unique participants and repeat sessions for each experiment. Below, we provide a description of data quality and example results from each of the various experiments.

3.1. Psychophysical & fMRI results

We defined a set of data quality metrics for our psychophysical and fMRI task experiments based on *a priori* thresholds for poor task performance. These included excessive head motion or failing to respond during fMRI tasks, and low accuracy during psychophysical catch trials. In general, the data we collected were of good quality as measured by these metrics, with 87% of our > 700 psychophysical and fMRI data sets passing quality control checks (Fig. 6; green bar). Statistical comparisons of these quality metrics are provided in Supplemental Table 5. Summaries of data quality metrics for each participant group in each experiment are presented in Supplemental Fig. 3 (psychophysics) & Supplemental Fig. 4 (fMRI). Data quality and example results for each of the experiments are described below. In Supplemental Fig. 5 we provide additional information regarding our fMRI data (the average head motion per TR, as well as temporal outliers per TR, across both groups and experiments). A chart detailing data quality for each experimental session in each participant is provided in Supplemental Fig. 6.

3.1.1. pRF results—Our population receptive field (pRF) mapping fMRI experiment used sweeping bars as visual stimuli to permit retinotopic mapping, as well as auditory tone sweeps and a motor tapping task. The top row of Fig. 7 shows retinotopic polar angle (A) and eccentricity (B) maps from one individual as well as a group of $n = 49$ control participants (C & D). Visual stimuli were presented at two different temporal frequencies (2 and 12 Hz), which permitted functional examination of temporal frequency selectivity across visual cortex (Fig. 7E-H). Our auditory tone sweep sequences (250–4000 Hz) also enabled tonotopic mapping in auditory cortical regions (Fig. 7I-L). Our motor tapping task involved rhythmic tapping of 5 body parts, with cue images presented at fixation (left and right thumbs, left and right toes, and tongue; see Methods). This permitted the functional identification of somatomotor cortical regions that were responsive during the tapping task (Fig. 7M-O). Data quality in our pRF experiment, as assessed by head motion and behavioral response rate, was generally high (Supplemental Fig. 4, left column), but differed significantly across groups (Supplemental Table 5), and was lowest among PwPP.

3.1.2. CSS results—Our contrast surround suppression (CSS) experiment permitted us to examine two visual phenomena: contrast-response functions and surround suppression. To this end, we acquired both psychophysical and 7 T fMRI data during a CSS task. Example CSS psychometric data are shown in Fig. 8A, which illustrates how contrast discrimination thresholds were defined from our psychophysical data. Threshold versus contrast data from control participants ($n = 32$) are shown in Fig. 8B, and illustrate the expected 'dipper' shape (open symbols); thresholds decrease slightly between pedestal contrasts of 0% (detection) and 0.6%, before increasing again at higher pedestal values. Further, there is a clear surround suppression effect in the 10% contrast pedestal data (the only with-surround pedestal condition we examined in the behavioral dataset): contrast discrimination thresholds are higher with versus without surrounding stimuli (Fig. 8B; filled vs. open symbols), indicating surround suppression of contrast perception.

An example ROI in primary visual cortex (V1) from the CSS fMRI task in a single participant is shown in Fig. 8C. The differential (i.e., center vs. surround) localizer produced the expected retinotopic activation pattern on the V1 cortical surface, with voxels that respond selectively to the center stimuli (green) surrounded by voxels responding to the surround (blue). 7 T fMRI responses in V1 from controls ($n = 36$) are shown in Fig. 8D. These data show the expected increase in V1 fMRI responses with increasing stimulus contrast, as well as the expected surround suppression effect; V1 fMRI responses from center-selective ROIs are lower with versus without surrounding stimuli (Fig. 8D; filled versus open symbols). Data quality in the CSS task, as assessed by psychophysical catch trials, fMRI head motion, and fMRI behavioral task responses, was generally high (Supplemental Figure 3 & Supplemental Fig. 4), but was significantly different across groups (Supplemental Table 5), and lowest among PwPP.

3.1.3. COP results—We acquired psychophysical (outside the scanner) and 7 T fMRI data during a contour object perception (COP) task. The degree of collinearity (i.e., orientation jitter) among Gabor contour elements and the presence or absence of irrelevant background elements were manipulated in order to examine contour integration and figure-ground segmentation (see Methods). Fig. 9A shows an example psychometric function from the COP task, which illustrates how decreasing contour jitter was associated with higher shape discrimination accuracy, as well as how jitter thresholds (70% accuracy) were quantified. Threshold data from a group of $n = 33$ control participants are shown in Fig. 9B. Fig. 9C shows an example ROI identified using the COP localizer data in right V1 from a single participant. As expected, the COP localizer yields a stripe of activation across V1 (orange), roughly perpendicular to the calcarine sulcus. In Fig. 9D, we show an example of 7 T fMRI responses from V1 in $n = 30$ controls across our 4 COP task conditions. This illustrates that the addition of background stimuli yielded higher fMRI responses (as would be expected with a larger number of stimuli on the screen), whereas contour jitter had little effect on the V1 fMRI response amplitude. We saw high data quality overall in our COP experiments (Supplemental Figs. 3 and 4), as assessed by psychophysical catch trials, fMRI head motion, and fMRI behavioral task responses. Of these, only head motion differed significantly across groups (Supplemental Table 5) and was highest (worst) among PwPP.

3.1.4. SFM results—We obtained psychophysical (but not fMRI) data from a structure-from-motion (SFM) task using the bi-stable rotating cylinder illusion. This task provided us with a behavioral measure of the stability of visual motion and form integration during the perception of a bi-stable illusion. Participants reported the perceived direction of rotation (clockwise or counterclockwise in depth) for an array of dots without explicit depth cues. This bi-stable stimulus yielded spontaneous alternations in the perceived direction of rotation. Example behavioral responses time courses from $n = 32$ healthy control participants are shown in Fig. 10A. In Fig. 10B, we show the average switch rates within the same group. On average, percept direction alternated about every 10 s, but there was substantial variability in bi-stable switch rates between individuals, as expected. Participants also completed a 'real switch' task as an experimental control condition, in which explicit depth cues were used to define physical changes in the rotation direction of the stimulus. A fair number of participants showed poor behavioral performance on the real switch task, which we interpret as difficulty in understanding and performing the task as instructed. Participants with poor performance were excluded from our analyses (see Methods). Performance in the SFM real switch task did not differ significantly across groups (Supplemental Table 5).

3.2. MRS results

To assess data quality in our MRS experiments, we defined a set of quality metrics, both *a priori* (linewidth of the unsuppressed water peak) and *post hoc* (spectrum linewidth and SNR). We observed high quality overall in our MRS data, with 92% of all of our > 300 MRS data sets passing all quality thresholds (Fig. 11; green bar). MRS data quality metrics for each group and VOI are shown in Supplemental Fig. 7, which indicates that data quality is generally comparable across groups and VOIs (Supplemental Table 6 shows statistical comparisons between groups for MRS quality metrics). A detailed summary of data quality for each VOI from each MRS scanning session in all participants is shown in Supplemental Fig. 8.

Example MR spectra from individual participants in both OCC and PFC VOIs are shown in Fig. 12A & C, respectively. Here we show example spectra (black) fit by LCModel (red), and the residual error after fitting, to illustrate the fit quality. Example voxel placement, and the proportion of gray matter, white matter, and CSF within each voxel are also illustrated. We fit a combination of 18 different metabolites using LCModel (see Supplemental Information for more details); examples of individual fits for glutamate and GABA are shown at the bottom of Fig. 12A & C.

To visualize the consistency of voxel placement across participants, we transformed voxel masks for each VOI in each scanning session into MNI canonical space, and then computed the percent overlap in space across participants and sessions. This is shown for both OCC and PFC voxels in Fig. 12B & D, respectively, and indicates a fairly high degree of consistency in voxel placement across individuals.

Finally, in Fig. 13 we show the quantification of glutamate (A) and GABA (B) in both OCC and PFC voxels across controls ($n = 42$ in OCC, 30 in PFC; fewer PFC data sets were collected due to a delay in hardware availability, as noted in the Methods). These plots

illustrate that metabolite concentrations, scaled relative to water, are within the expected range for our healthy adult population, as measured by this MRS technique (Marjańska et al., 2017). We note that previous studies have also observed numerically higher glutamate levels in prefrontal as compared to occipital cortex (Marsman et al., 2014; Zhang and Shen, 2015), though such differences were not statistically significant.

4. Discussion

This report of the data collected as part of our Psychosis HCP project is intended to facilitate the use of this dataset by the research community. We are pleased that, overall, this project yielded a substantial number of data sets, and relatively few were hampered by the expected confounds of head motion, fatigue, difficulty complying with task instructions, or equipment malfunction. For this report, we have included results of analyses that extract a small number behavioral or physiological parameters from a subset of control participants, in order to provide a sense of effect sizes and measurement error in the dataset. No results from PwPP or relatives are included in this report; more thorough analyses of these datasets will be included in future publications focused on the findings from group comparisons. The primary goal of this report is to document methods and promote the availability of this dataset.

This dataset is one of many available through db.humanconnectome.org as part of the Human Connectome Project. In addition to the 7 T visual pRF data acquired as part of the original Young Adult HCP (Benson et al., 2018), other HCP studies have focused on the structure and function of the visual system in conditions such as macular degeneration, low vision, blindness, and sight restoration. Further HCP data that are relevant to the current study are available from other projects focused on topics including early psychosis and the genetic basis of mental disorders (e.g., Amish Connectome).

We have reported here only on experiments performed during visits for 7 T scanning sessions. Our 3 T dataset has been described in a previous publication (Demro et al., 2021). All participants at 7 T also participated in 3 T scanning sessions, and although we have not detailed the potential approaches in this report, it is entirely feasible to design analyses that integrate 3 T resting state or cortical parcellation derived from 3 T data with functional responses or neurotransmitter concentrations measured at 7 T. Thus, we hope that this multimodal dataset, once fully released in 2023, will provide the basis for many multimodal analyses by diverse research groups.

Because symptoms vary over time for PwPP, and performance on visual tasks such as contour object perception has been found to correlate with symptom severity (Keane et al., 2018; Silverstein et al., 2000), a subset of PwPP participating in this study were scanned on 2 occasions, separated by at least 1 month. Although not all PwPP returned for a second visit, we successfully obtained 39 pairs of repeat datasets in this group. The BPRS, SANS, and SAPS were collected at both 7 T visits, to provide a snapshot of clinical symptomatology that can be analyzed in conjunction with visual task performance, fMRI responses, and prefrontal or occipital metabolite concentrations. The goal of this aspect of

the project is to provide data that may help elucidate the neural changes underlying shifts in symptom levels and visual task performance.

Naturally, acquiring a dataset this size is not without challenges, particularly when the project coincides with a worldwide viral pandemic. We have provided detailed information in the Methods and Supplemental Information describing which datasets are complete and incomplete, and which experimental protocols were changed over time. The authors are more than happy to consult with potential users of this dataset to help them navigate the details of exactly which data are available for which subsets of participants and experiments.

In sum, this dataset offers novel opportunities to investigate specific neurophysiological responses during visual experiments designed to study particular neural mechanisms (e.g., contour facilitation, contrast surround suppression) among PwPP, their relatives, and healthy controls, both cross-sectionally and across time. Our data may also facilitate investigating the role of neurochemical functioning (via MRS) in these groups. Researchers may also wish to explore relationships with structural and resting state functional connectivity measures acquired in the same participants at 3 T (Demro et al., 2021). For each usage case, approximately 150–200 high-quality datasets (including repeated scans) are publicly available to support future analyses. We know of very few other 7 T fMRI or MRS data sets that are currently publicly available, and even fewer that are designed to investigate visual functioning (Allen et al., 2022; Benson et al., 2018; Sengupta et al., 2017) and / or psychotic psychopathology.

5. Conclusion

We show that it is feasible to collect a diverse array of high quality brain imaging data in visual cortex at ultra-high field (7 tesla) from a relatively large sample of healthy controls ($N = 43$), biological relatives ($N = 44$), and PwPP ($N = 66$) at a single research site. We demonstrate how cutting-edge multimodal imaging and behavioral methods can be applied to investigate visual neurophysiology in PwPP. By applying visual neuroscience methods along with standardized imaging methods from the Human Connectome Project (Benson et al., 2018; Glasser et al., 2016; Van Essen et al., 2013), our datasets offer new opportunities to investigate the role(s) of structural and functional connectivity in abnormal visual processing among PwPP. Hypotheses of neural dysfunction in PwPP that might be examined include a disruption in the balance of excitation and inhibition (Foss-Feig et al., 2017; Lewis et al., 2005; Lisman, 2012; Moghaddam and Javitt, 2012), thalamo-cortical dysconnectivity (Anticevic et al., 2014; Cheng et al., 2015; Damaraju et al., 2014; Dong et al., 2019; Giraldo-Chica and Woodward, 2017; Ramsay, 2019; Ramsay et al., 2017), abnormal visual gain control (Butler et al., 2008; Phillips and Silverstein, 2013), impaired top-down attentional modulation (Gold et al., 2018; Luck et al., 2019a, 2019b), and disrupted predictive coding (Adams et al., 2013; Horga and Abi-Dargham, 2019; Sterzer et al., 2018). In summary, our goal is to provide sufficient information to facilitate subsequent investigations of visual processing in PwPP using the data, code, and resources that we have made available as part of the Psychosis Human Connectome Project. We invite interested researchers to reach out to us for collaboration and support.

Supplementary Material

Refer to Web version on PubMed Central for supplementary material.

Acknowledgments

This work was supported by funding from the National Institutes of Health (U01 MH108150). Salary support for MPS was provided in part by K01 MH120278, and salary support for CAO was provided in part by R01 MH111447. Support for MR scanning at the University of Minnesota Center for Magnetic Resonance Research was provided by P41 EB015894 and P30 NS076408. This work used tools from the University of Minnesota Clinical and Translational Science Institute that were supported by UL1 TR002494.

Data availability

Our data and code are available through the links included in our manuscript.

References

Adams RA, Stephan KE, Brown HR, Frith CD, Friston KJ, 2013. The computational anatomy of psychosis. Front. Psychiatry 4.

Allen EJ, St-Yves G, Wu Y, Breedlove JL, Prince JS, Dowdle LT, Nau M, Caron B, Pestilli F, Charest I, Hutchinson JB, Naselaris T, Kay K, 2022. A massive 7T fMRI dataset to bridge cognitive neuroscience and artificial intelligence. Nat. Neurosci 25, 116–126. [PubMed: 34916659]

Andreasen NC, 1982. Negative symptoms in schizophrenia: Definition and reliability. Arch. Gen. Psychiatry 39, 784–788. [PubMed: 7165477]

Andreasen NC, 1984. Scale for the Assessment of Positive Symptoms. University of Iowa, Iowa City, IA.

Anticevic A, Cole MW, Repovs G, Murray JD, Brumbaugh MS, Winkler AM, Savic A, Krystal JH, Pearlson GD, Glahn DC, 2014. Characterizing thalamo-cortical disturbances in schizophrenia and bipolar illness. Cereb. Cortex 24, 3116–3130. [PubMed: 23825317]

Arditi A, 2005. Improving the design of the letter contrast sensitivity test. Investig. Opthalmol. Vis. Sci 46, 2225.

Benson NC, Jamison KW, Arcaro MJ, Vu AT, Glasser MF, Coalson TS, Van Essen DC, Yacoub E, Ugurbil K, Winawer J, Kay K, 2018. The Human Connectome Project 7 Tesla retinotopy dataset: Description and population receptive field analysis. J. Vis 18, 23.

Bonilha L, Molnar C, Horner MD, Anderson B, Forster L, George MS, Nahas Z, 2008. Neurocognitive deficits and prefrontal cortical atrophy in patients with schizophrenia. Schizophr. Res 101, 142–151. [PubMed: 18164594]

Boynton GM, Demb JB, Glover GH, Heeger DJ, 1999. Neuronal basis of contrast discrimination. Vis. Res 39, 257–269. [PubMed: 10326134]

Butler PD, Silverstein S, Dakin SC, 2008. Visual perception and its impairment in schizophrenia. Biol. Psychiatry 64, 40–47. [PubMed: 18549875]

Calkins ME, Iacono WG, Ones DS, 2008. Eye movement dysfunction in first-degree relatives of patients with schizophrenia: A meta-analytic evaluation of candidate endophenotypes. Brain Cogn. 68, 436–461. [PubMed: 18930572]

Cardno AG, Marshall EJ, Coid B, Macdonald AM, Ribchester TR, Davies NJ, Venturi P, Jones LA, Lewis SW, Sham PC, Gottesman II, Farmer AE, McGuffin P, Reveley AM, Murray RM, 1999. Heritability estimates for psychotic disorders: The maudsley twin psychosis series. Arch. Gen. Psychiatry 56, 162. [PubMed: 10025441]

Cardno AG, Owen MJ, 2014. Genetic relationships between schizophrenia, bipolar disorder, and schizoaffective disorder. Schizophr. Bull 40, 504–515. [PubMed: 24567502]

Cavelier P, Hamann M, Rossi D, Mobbs P, Attwell D, 2005. Tonic excitation and inhibition of neurons: Ambient transmitter sources and computational consequences. Prog. Biophys. Mol. Biol. 87, 3–16. [PubMed: 15471587]

Cheng W, Palaniyappan L, Li M, Kendrick KM, Zhang J, Luo Q, Liu Z, Yu R, Deng W, Wang Q, Ma X, Guo W, Francis S, Liddle P, Mayer AR, Schumann G, Li T, Feng J, 2015. Voxel-based, brain-wide association study of aberrant functional connectivity in schizophrenia implicates thalamocortical circuitry. NPJ Schizophr. 1.

Chkonia E, Roinishvili M, Makhatadze N, Tsverava L, Stroux A, Neumann K, Herzog MH, Brand A, 2010. The shine-through masking paradigm is a potential endophenotype of schizophrenia. PLoS One 5, e14268. [PubMed: 21151559]

Cudalbu C, Behar KL, Bhattacharyya PK, Bogner W, Borbath T, Graaf RA, Gruetter R, Henning A, Juchem C, Kreis R, Lee P, Lei H, Marjańska M, Mekle R, Murali-Manohar S, Považan M, Rackayová V, Simicic D, Slotboom J, Soher BJ, Starčuk Z, Starčuková J, Tkáč I, Williams S, Wilson M, Wright AM, Xin L, Mlynárik V, 2021. Contribution of macromolecules to brain ^{1}H MR spectra: Experts' consensus recommendations. NMR Biomed. 34.

Cuthbert BN, 2014. The RDoC framework: Facilitating transition from ICD/DSM to dimensional approaches that integrate neuroscience and psychopathology: forum - the research domain criteria project. World Psychiatry 13, 28–35. [PubMed: 24497240]

Da Costa S, van der Zwaag W, Marques JP, Frackowiak RSJ, Clarke S, Saenz M, 2011. Human primary auditory cortex follows the shape of Heschl's gyrus. J. Neurosci 31, 14067–14075. [PubMed: 21976491]

Damaraju E, Allen EA, Belger A, Ford JM, McEwen S, Mathalon DH, Mueller BA, Pearlson GD, Potkin SG, Preda A, Turner JA, Vaidya JG, van Erp TG, Calhoun VD, 2014. Dynamic functional connectivity analysis reveals transient states of dysconnectivity in schizophrenia. NeuroImage Clin. 5, 298–308. [PubMed: 25161896]

Demro C, Mueller BA, Kent JS, Burton PC, Olman CA, Schallmo MP, Lim KO, Sponheim SR, 2021. The psychosis human connectome project: An overview. NeuroImage 241, 118439. [PubMed: 34339830]

Dong D, Duan M, Wang Y, Zhang X, Jia X, Li Y, Xin F, Yao D, Luo C, 2019. Reconfiguration of dynamic functional connectivity in sensory and perceptual system in schizophrenia. Cereb. Cortex 29, 3577–3589. [PubMed: 30272139]

Dumoulin SO, Wandell BA, 2008. Population receptive field estimates in human visual cortex. NeuroImage 39, 647–660. [PubMed: 17977024]

Egerton A, Modinos G, Ferrera D, McGuire P, 2017. Neuroimaging studies of GABA in schizophrenia: A systematic review with meta-analysis. Transl. Psychiatry 7, e1147. [PubMed: 28585933]

Engel S, 1997. Retinotopic organization in human visual cortex and the spatial precision of functional MRI. Cereb. Cortex 7, 181–192. [PubMed: 9087826]

Featherstone DE, 2010. Intercellular glutamate signaling in the nervous system and beyond. ACS Chem. Neurosci 1, 4–12. [PubMed: 22778802]

First MB, 1997. User's Guide for the Structured Clinical Interview for DSM-IV Axis I Disorders SCID-I: Clinician Version. American Psychiatric Publishing, Inc.

Foss-Feig JH, Adkinson BD, Ji JL, Yang G, Srihari VH, McPartland JC, Krystal JH, Murray JD, Anticevic A, 2017. Searching for cross-diagnostic convergence: Neural mechanisms governing excitation and inhibition balance in schizophrenia and autism spectrum disorders. Biol. Psychiatry 81, 848–861. [PubMed: 28434615]

Garcia-Perez MA, 1998. Forced-choice staircases with fixed step sizes: Asymptotic and small-sample properties. Vis. Res 38, 1861–1881. [PubMed: 9797963]

Giraldo-Chica M, Woodward ND, 2017. Review of thalamocortical resting-state fMRI studies in schizophrenia. Schizophr. Res 180, 58–63. [PubMed: 27531067]

Glasser MF, Smith SM, Marcus DS, Andersson JLR, Auerbach EJ, Behrens TEJ, Coalson TS, Harms MP, Jenkinson M, Moeller S, Robinson EC, Sotiropoulos SN, Xu J, Yacoub E, Ugurbil K, Van Essen DC, 2016. The Human Connectome Project's neuroimaging approach. Nature neuroscience 19, 1175–1187. [PubMed: 27571196]

Godlewska BR, Clare S, Cowen PJ, Emir UE, 2017. Ultra-high-field magnetic resonance spectroscopy in psychiatry. Front. Psychiatry 8, 123. [PubMed: 28744229]

Gold JM, Robinson B, Leonard CJ, Hahn B, Chen S, McMahon RP, Luck SJ, 2018. Selective attention, working memory, and executive function as potential independent sources of cognitive dysfunction in schizophrenia. Schizophr. Bull 44, 1227–1234. [PubMed: 29140504]

Gonzalez-Burgos G, Lewis DA, 2008. GABA neurons and the mechanisms of network oscillations: Implications for understanding cortical dysfunction in schizophrenia. Schizophr. Bull 34, 944–961. [PubMed: 18586694]

Gottesman II, Gould TD, 2003. The endophenotype concept in psychiatry: Etymology and strategic intentions. Am. J. Psychiatry 160, 636–645. [PubMed: 12668349]

Gruetter R, 1993. Automatic, localized *in vivo* adjustment of all first-and second-order shim coils. Magn. Reson. Med 29, 804–811. [PubMed: 8350724]

Gruetter R, Tkáč I, 2000. Field mapping without reference scan using asymmetric echo–planar techniques. Magn. Reson. Med 43, 319–323. [PubMed: 10680699]

Hashimoto T, Bazmi HH, Mirnics K, Wu Q, Sampson AR, Lewis DA, 2008. Conserved regional patterns of GABA-related transcript expression in the neocortex of subjects with schizophrenia. Am. J. Psychiatry 165, 479–489. [PubMed: 18281411]

Hetrick WP, Erickson MA, Smith DA, 2012. Phenomenological dimensions of sensory gating. Schizophr. Bull 38, 178–191. [PubMed: 20525773]

Horga G, Abi-Dargham A, 2019. An integrative framework for perceptual disturbances in psychosis. Nat. Rev. Neurosci 20, 763–778. [PubMed: 31712782]

Hubel DH, Wiesel TN, 1962. Receptive fields, binocular integration and functional architecture in the cat's visual cortex. J. Physiol 160, 106–154. [PubMed: 14449617]

Iacono WG, Malone SM, Vrieze SI, 2017. Endophenotype best practices. Int. J. Psychophysiol 111, 115–144. [PubMed: 27473600]

Javitt DC, 2004. Glutamate as a therapeutic target in psychiatric disorders. Mol. Psychiatry 9, 984–997. [PubMed: 15278097]

Jeste DV, Palmer BW, Appelbaum PS, Golshan S, Glorioso D, Dunn LB, Kim K, Meeks T, Kraemer HC, 2007. A new brief instrument for assessing decisional capacity for clinical research. Arch. Gen. Psychiatry 64, 966–974. [PubMed: 17679641]

Keane BP, Paterno D, Kastner S, Krekelberg B, Silverstein SM, 2018. Intact illusory contour formation but equivalently impaired visual shape completion in first- and later-episode schizophrenia. J. Abnorm. Psychol 128, 57–68. [PubMed: 30346202]

Keefe RSE, Goldberg TE, Harvey PD, Gold J, Poe MP, Coughenour L, 1999. Brief assessment of cognition in schizophrenia. Schizophr. Res..

Kelemen O, Kiss I, Benedek G, Keri S, 2013. Perceptual and cognitive effects of antipsychotics i n first-episode schizophrenia: The potential imact of GABA concentration in the visual cortex. Prog. Neuro Psychopharmacol. Biol. Psychiatry 47, 13–19.

Kéri S, Kelemen O, Benedek G, Janka Z, 2001. Different trait markers for schizophrenia and bipolar disorder: A neurocognitive approach. Psychol. Med 31, 915–922. [PubMed: 11459389]

King DJ, Hodgekins J, Chouinard PA, Chouinard VA, Sperandio I, 2017. A review of abnormalities in the perception of visual illusions in schizophrenia. Psychon. Bull. Rev 24, 734–751. [PubMed: 27730532]

Kingdom FAA, Prins N, 2010. Psychophysics: A Practical I ntroduction. Academic Press, London.

Klein SD, Olman CA, Sponheim SR, 2020a. Perceptual mechanisms of visual hallucinations and illusions in psychosis. J. Psychiatry Brain Sci 5, e200020.

Klein SD, Shekels LL, McGuire KA, Sponheim SR, 2020b. Neural anomalies during vigilance in schizophrenia: diagnostic specificity and genetic associations. NeuroImage Clin. 28, 102414. [PubMed: 32950905]

Koo TK, Li MY, 2016. A guideline of selecting and reporting intraclass correlation coefficients for reliability research. J. Chiropr. Med 15, 155–163. [PubMed: 27330520]

Kotov R, Krueger RF, Watson D, Achenbach TM, Althoff RR, Bagby RM, Brown TA, Carpenter WT, Caspi A, Clark LA, Eaton NR, Forbes MK, Forbush KT, Goldberg D, Hasin D, Hyman SE, Ivanova MY, Lynam DR, Markon K, Miller JD, Moffitt TE, Morey LC, Mullins-Sweatt SN, Ormel J, Patrick CJ, Regier DA, Rescorla L, Ruggero CJ, Samuel DB, Sellbom M, Simms LJ, Skodol AE, Slade T, South SC, Tackett JL, Waldman ID, Waszczuk MA, Widiger TA, Wright AGC,

Zimmerman M, 2017. The hierarchical taxonomy of psychopathology (HiTOP): A dimensional alternative to traditional nosologies. J. Abnorm. Psychol 126, 454–477. [PubMed: 28333488]

Kriegeskorte N, Mur M, Ruff DA, Kiani R, Bodurka J, Esteky H, Tanaka K, Bandettini PA, 2008. Matching categorical object representations in inferior temporal cortex of man and monkey. Neuron 60, 1126–1141. [PubMed: 19109916]

Krueger RF, Derringer J, Markon KE, Watson D, Skodol AE, 2012. Initial construction of a maladaptive personality trait model and inventory for DSM-5. Psychol. Med 42, 1879–1890. [PubMed: 22153017]

Kumar J, Liddle EB, Fernandes CC, Palaniyappan L, Hall EL, Robson SE, Simmonite M, Fiesal J, Katshu MZ, Qureshi A, Skelton M, Christodoulou NG, Brookes MJ, Morris PG, Liddle PF, 2020. Glutathione and glutamate in schizophrenia: A 7T MRS study. Mol. Psychiatry 25, 873–882. [PubMed: 29934548]

Legge GE, Foley JM, 1980. Contrast masking in human vision. J. Opt. Soc. Am 70, 1458–1471. [PubMed: 7463185]

Lewis DA, Hashimoto T, Volk DW, 2005. Cortical inhibitory neurons and schizophrenia. Nat. Rev. Neurosci 6, 312–324. [PubMed: 15803162]

Lin A, Andronesi O, Bogner W, Choi IY, Coello E, Cudalbu C, Juchem C, Kemp GJ, Kreis R, Kršňák M, Lee P, Maudsley AA, Meyerspeer M, Mlynarik V, Near J, Öz G, Peek AL, Puts NA, Ratai EM, Tkáč I, Mullins PG, 2021. Minimum reporting standards for *in vivo* magnetic resonance spectroscopy (MRSinMRS): Experts' consensus recommendations. NMR Biomed. 34, e4484. [PubMed: 33559967]

Lisman J, 2012. Excitation, inhibition, local oscillations, or large-scale loops: What causes the symptoms of schizophrenia? Curr. Opin. Neurobiol 22, 537–544. [PubMed: 22079494]

Lotze M, Erb M, Flor H, Huelsmann E, Godde B, Grodd W, 2000. fMRI evaluation of somatotopic representation in human primary motor cortex. NeuroImage 11, 473–481. [PubMed: 10806033]

Luck SJ, Hahn B, Leonard CJ, Gold JM, 2019a. The hyperfocusing hypothesis: a new account of cognitive dysfunction in schizophrenia. Schizophr. Bull 45, 991–1000. [PubMed: 31317191]

Luck SJ, Leonard CJ, Hahn B, Gold JM, 2019b. Is attentional filtering impaired in schizophrenia? Schizophr. Bull 45, 1001–1011. [PubMed: 31206163]

Marjańska M, McCarten JR, Hodges J, Hemmy LS, Grant A, Deelchand DK, Terpstra M, 2017. Region-specific aging of the human brain as evidenced by neurochemical profiles measured noninvasively in the posterior cingulate cortex and the occipital lobe using 1H magnetic resonance spectroscopy at 7 T. Neuroscience 354, 168–177. [PubMed: 28476320]

Markon KE, Chmielewski M, Miller CJ, 2011. The reliability and validity of discrete and continuous measures of psychopathology: A quantitative review. Psychol. Bull 137, 856–879. [PubMed: 21574681]

Marsman A, Mandl RCW, Klomp DWJ, Bohlken MM, Boer VO, Andreychenko A, Cahn W, Kahn RS, Luijten PR, Hulshoff Pol HE, 2014. GABA and glutamate in schizophrenia: A 7 T 1H-MRS study. NeuroImage Clin. 6, 398–407. [PubMed: 25379453]

Matsuzawa D, Obata T, Shirayama Y, Nonaka H, Kanazawa Y, Yoshitome E, Takanashi J, Matsuda T, Shimizu E, Ikehira H, Iyo M, Hashimoto K, 2008. Negative correlation between brain glutathione level and negative symptoms in schizophrenia: A 3T 1H-MRS study. PLoS One 3, e1944. [PubMed: 18398470]

Mescher M, Merkle H, Kirsch J, Garwood M, Gruetter R, 1998. Simultaneous *in vivo* spectral editing and water suppression. NMR Biomed. 11, 266–272. [PubMed: 9802468]

Moerel M, De Martino F, Formisano E, 2014. An anatomical and functional topography of human auditory cortical areas. Front. Neurosci 8.

Moghaddam B, Javitt D, 2012. From revolution to evolution: the glutamate hypothesis of schizophrenia and its implication for treatment. Neuropsychopharmacology 37, 4–15. [PubMed: 21956446]

Norman-Haignere S, Kanwisher N, McDermott JH, 2013. Cortical pitch regions in humans respond primarily to resolved harmonics and are located in specific tonotopic regions of anterior auditory cortex. J. Neurosci 33, 19451–19469. [PubMed: 24336712]

Notredame CE, Pins D, Deneve S, Jardri R, 2014. What visual illusions teach us about schizophrenia. Front. Integr. Neurosc 8, 63.

Olman CA, Inati S, Heeger DJ, 2007. The effect of large veins on spatial localization with GE BOLD at 3 T: Displacement, not blurring. NeuroImage 34, 1126–1135. [PubMed: 17157534]

Olman CA, Pickett KA, Schallmo M-P, Kimberley TJ, 2012. Selective BOLD responses to individual finger movement measured with fMRI at 3T. Hum. Brain Mapp 33, 1594–1606. [PubMed: 21674691]

Öngür D, Prescot AP, Jensen JE, Rouse ED, Cohen BM, Renshaw PF, Olson DP, 2010a. T_2 relaxation time abnormalities in bipolar disorder and schizophrenia: T_2 in bipolar disorder and schizophrenia. Magn. Reson. Med 63, 1–8. [PubMed: 19918902]

Öngür D, Prescot AP, McCarthy J, Cohen BM, Renshaw PF, 2010b. Elevated gamma-aminobutyric acid levels in chronic schizophrenia. Biol. Psychiatry 68, 667–670. [PubMed: 20598290]

Peirce JW, 2007. PsychoPy—psychophysics software in python. J. Neurosci. Methods 162, 8–13 . [PubMed: 17254636]

Perkins DO, Jeffries CD, Do KQ, 2020. Potential roles of redox dysregulation in the development of schizophrenia. Biol. Psychiatry 88, 326–336. [PubMed: 32560962]

Phillips WA, Silverstein SM, 2013. The coherent organization of mental life depends on mechanisms for context-sensitive gain-control that are impaired in schizophrenia. Front. Psychol 4, 307. [PubMed: 23755035]

Pokorny VJ, Espensen-Sturges TD, Burton PC, Sponheim SR, Olman CA, 2021a. Aberrant cortical connectivity during ambiguous object recognition is associated with schizophrenia. Biol. Psychiatry Cogn. Neurosci. Neuroimaging 6, 1193–1201. [PubMed: 33359154]

Pokorny VJ, Lano TJ, Schallmo MP, Olman CA, Sponheim SR, 2021b. Reduced influence of perceptual context in schizophrenia: behavioral and neurophysiological evidence. Psychol. Med 51, 786–794. [PubMed: 31858929]

Qiu C, Burton PC, Kersten D, Olman CA, 2016. Responses in early visual areas to contour integration are context dependent. J. Vis 16, 19.

Rae CD, 2014. A guide to the metabolic pathways and function of metabolites observed in human brain 1H magnetic resonance spectra. Neurochem. Res 39, 1–36. [PubMed: 24258018]

Raine A, 1991. The SPQ: A scale for the assessment of schizotypal personality based on DSM-III-R criteria. Schizophr. Bull 17, 555–564. [PubMed: 1805349]

Ramsay IS, 2019. An activation likelihood estimate meta-analysis of thalamocortical dysconnectivity in psychosis. Biol. Psychiatry Cogn. Neurosci. Neuroimaging 4, 859–869. [PubMed: 31202821]

Ramsay IS, Nienow TM, MacDonald AW, 2017. Increases in intrinsic thalamocortical connectivity and overall cognition following cognitive remediation in chronic schizophrenia. Biol. Psychiatry Cogn. Neurosci. Neuroimaging 2, 355–362. [PubMed: 28584882]

Rowland LM, Kontson K, West J, Edden RA, Zhu H, Wijtenburg SA, Holcomb HH, Barker PB, 2013. *In vivo* measurements of glutamate, GABA, and NAAG in schizophrenia. Schizophr. Bull 39, 1096–1104. [PubMed: 23081992]

Salavati B, Rajji TK, Price R, Sun Y, Graff-Guerrero A, Daskalakis ZJ, 2014. Imaging-based neurochemistry in schizophrenia: A systematic review and implications for dysfunctional long-term potentiation. Schizophr. Bull 41, 44–56. [PubMed: 25249654]

Schallmo MP, Grant AN, Burton PC, Olman CA, 2016. The effects of orientation and attention during surround suppression of small image features: A 7 Tesla fMRI study. J. Vis 16, 19.

Schallmo MP, Kale AM, Millin R, Flevaris AV, Brkanac Z, Edden RAE, Bernier RA, Murray SO, 2018. Suppression and facilitation of human neural responses. eLife 7, e30334. [PubMed: 29376822]

Schallmo MP, Kolodny T, Kale AM, Millin R, Flevaris AV, Edden RAE, Gerdts J, Bernier RA, Murray SO, 2020. Weaker neural suppression in autism. Nat. Commun 11, 2675. [PubMed: 32472088]

Schallmo MP, Sponheim SR, Olman CA, 2013. Abnormal contextual modulation of visual contour detection in patients with schizophrenia. PLoS One 8, e68090. [PubMed: 23922637]

Schallmo MP, Sponheim SR, Olman CA, 2015. Reduced contextual effects on visual contrast perception in schizophrenia and bipolar affective disorder. Psychol. Med 45, 3527–3537. [PubMed: 26315020]

Schallmo MP, Weldon KB, Burton PC, Sponheim SR, Olman CA, 2021. Assessing methods for geometric distortion compensation in 7 T gradient echo functional MRI data. Hum. Brain Mapp 42, 4205–4223. [PubMed: 34156132]

Schousboe A, Sonnewald U, 2016. The Glutamate/GABA-Glutamine Cycle: Amino Acid Neurotransmitter Homeostasis. Springer International Publishing, Cham, Switzerland.

Sengupta A, Yakupov R, Speck O, Pollmann S, Hanke M, 2017. Ultra high-field (7 T) multi-resolution fMRI data for orientation decoding in visual cortex. Data Brief 13, 219–222. [PubMed: 28616455]

Silverstein S, Berten S, Essex B, Kovacs I, Susmaras T, Little DM, 2009. An fMRI examination of visual integration in schizophrenia. J. Integr. Neurosci 8, 175–202. [PubMed: 19618486]

Silverstein S, Hatashita-Wong M, Schenkel L, Wilkniss S, Kovacs I, Feher A, Smith T, Goicochea C, Uhlhaas P, Carpiniello K, 2006. Reduced top-down influences in contour detection in schizophrenia. Cogn. Neuropsychiatry 11, 112–132. [PubMed: 16537237]

Silverstein SM, Harms MP, Carter CC, Gold JM, Keane BP, MacDonald A, Ragland JD, Barch DM, 2015. Cortical contributions to impaired contour integration in schizophrenia. Neuropsychologia 75, 469–480. [PubMed: 26160288]

Silverstein SM, Kovacs I, Corry R, Valone C, 2000. Perceptual organization, the disorganization syndrome, and context processing in chronic schizophrenia. Schizophr. Res 43, 11–20. [PubMed: 10828411]

Snellen H, 1862. Probebuchstaben zur Bestimmung der Sehschärfe.

Sponheim SR, McGuire KA, Stanwyck JJ, 2006. Neural anomalies during sustained attention in first-degree biological relatives of schizophrenia patients. Biol. Psychiatry 60, 242–252. [PubMed: 16460700]

Sterzer P, Adams RA, Fletcher P, Frith C, Lawrie SM, Muckli L, Petrovic P, Uhlhaas P, Voss M, Corlett PR, 2018. The predictive coding account of psychosis. Biol. Psychiatry 84, 634–643. [PubMed: 30007575]

Sydnor VJ, Roalf DR, 2020. A meta-analysis of ultra-high field glutamate, glutamine, GABA and glutathione 1HMRS in psychosis: Implications for studies of psychosis risk. Schizophr. Res 226, 61–69. [PubMed: 32723493]

Taylor SF, Tso IF, 2015. GABA abnormalities in schizophrenia: A methodological review of *in vivo* studies. Schizophr. Res 167, 84–90. [PubMed: 25458856]

Terpstra M, Cheong I, Lyu T, Deelchand DK, Emir UE, Bednařík P, Eberly LE, Öz G, 2016. Test-retest reproducibility of neurochemical profiles with short-echo, single-voxel MR spectroscopy at 3T and 7T. Magn. Reson. Med 76, 1083–1091. [PubMed: 26502373]

Thakkar KN, Rösler L, Wijnen JP, Boer VO, Klomp DWJ, Cahn W, Kahn RS, Neggers SFW, 2017. 7T proton magnetic resonance spectroscopy of gamma-aminobutyric acid, glutamate, and glutamine reveals altered concentrations in patients with schizophrenia and healthy siblings. Biol. Psychiatry 81, 525–535. [PubMed: 27316853]

Tkáč I, Andersen P, Adriany G, Merkle H, Ugurbil K, Gruetter R, 2001. *In vivo* 1H NMR spectroscopy of the human brain at 7 T. Magn. Reson. Med 46, 451–456. [PubMed: 11550235]

Treue S, Husain M, Andersen RA, 1991. Human perception of structure from motion. Vis. Res 31, 59–75. [PubMed: 2006555]

Tully LM, Lincoln SH, Liyanage-Don N, Hooker CI, 2014. Impaired cognitive control mediates the relationship between cortical thickness of the superior frontal gyrus and role functioning in schizophrenia. Schizophr. Res 152, 358–364. [PubMed: 24388000]

Ullman S, 1979. The interpretation of structure from motion. Proc. R. Soc. B Biol. Sci 203, 405–426. [PubMed: 34162]

Van Essen DC, Anderson CH, Felleman DJ, 1992. Information processing in the primate visual system: an integrated systems perspective. Science 255, 419–423. [PubMed: 1734518]

Van Essen DC, Smith SM, Barch DM, Behrens TEJ, Yacoub E, Ugurbil K, 2013. The WU-Minn human connectome project: an overview. NeuroImage 80, 62–79. [PubMed: 23684880]

Venkatraman V, Rosati AG, Taren AA, Huettel SA, 2009. Resolving response, decision, and strategic control: Evidence for a functional topography in dorsomedial prefrontal cortex. J. Neurosci 29, 13158–13164. [PubMed: 19846703]

Ventura J, Nuechterlein KH, Subotnik KL, Gutkind D, Gilbert EA, 2000. Symptom dimensions in recent-onset schizophrenia and mania: a principal components analysis of the 24-item brief psychiatric rating scale. Psychiatry Res. 97, 129–135. [PubMed: 11166085]

Vu A, Jamison K, Glasser MF, Smith SM, Coalson T, Moeller S, Auerbach EJ, Uğurbil K, Yacoub E, 2017. Tradeoffs in pushing the spatial resolution of fMRI for the 7T human connectome project. NeuroImage 154, 23–32. [PubMed: 27894889]

Vu AT, Auerbach E, Lenglet C, Moeller S, Sotiropoulos SN, Jbabdi S, Andersson J, Yacoub E, Ugurbil K, 2015. High resolution whole brain diffusion imaging at 7 T for the human connectome project. NeuroImage 122, 318–331. [PubMed: 26260428]

Waters F, Collerton D, ffytche DH, Jardri R, Pins D, Dudley R, Blom JD, Mosimann UP, Eperjesi F, Ford S, Larøi, F., 2014. Visual hallucinations in the psychosis spectrum and comparative information from neurodegenerative disorders and eye disease. Schizophr. Bull 40, S233–S245. [PubMed: 24936084]

Wechsler D, 2008. Wechsler Adult Intelligence Scale, 4th ed. Pearson Assessment, San Antonio, TX.

Wijtenburg SA, Yang S, Fischer BA, Rowland LM, 2015. *In vivo* assessment of neurotransmitters and modulators with magnetic resonance spectroscopy: Application to schizophrenia. Neurosci. Biobehav. Rev 51, 276–295. [PubMed: 25614132]

Wu Y, Wang W, Díez-Sampedro A, Richerson GB, 2007. Nonvesicular inhibitory neurotransmission via reversal of the GABA transporter GAT-1. Neuron 56, 851–865. [PubMed: 18054861]

Yeap S, Kelly SP, Sehatpour P, Magno E, Javitt DC, Garavan H, Thakore JH, Foxe JJ, 2006. Early visual sensory deficits as endophenotypes for schizophrenia. Arch. Gen. Psychiatry 63, 1180–1188. [PubMed: 17088498]

Yoon JH, Maddock RJ, DongBo Cui E, Minzenberg MJ, Niendam TA, Lesh T, Solomon M, Ragland JD, Carter C, 2020. Reduced *in vivo* visual cortex GABA in schizophrenia, a replication in a recent onset sample. Schizophr. Res 215, 217–222. [PubMed: 31704157]

Yoon JH, Maddock RJ, Rokem A, Silver MA, Minzenberg MJ, Ragland JD, Carter CS, 2010. GABA concentration is reduced in visual cortex in schizophrenia and correlates with orientation-specific surround suppression. J. Neurosci 30, 3777–3781. [PubMed: 20220012]

Yoon JH, Sheremata SL, Rokem A, Silver MA, 2013. Windows to the soul: Vision science as a tool for studying biological mechanisms of information processing deficits in schizophrenia. Front. Psychol 4, 681. [PubMed: 24198792]

Yu C, Klein SA, Levi DM, 2003. Cross- and iso-oriented surrounds modulate the contrast response function: The effect of surround contrast. J. Vis 3, 527–540. [PubMed: 14632605]

Zenger-Landolt B, Heeger DJ, 2003. Response suppression in V1 agrees with psychophysics of surround masking. J. Neurosci 23, 6884–6893. [PubMed: 12890783]

Zhang Y, Shen J, 2015. Regional and tissue-specific differences in brain glutamate concentration measured by *in vivo* single voxel MRS. J. Neurosci. Methods 239, 94–99. [PubMed: 25261738]

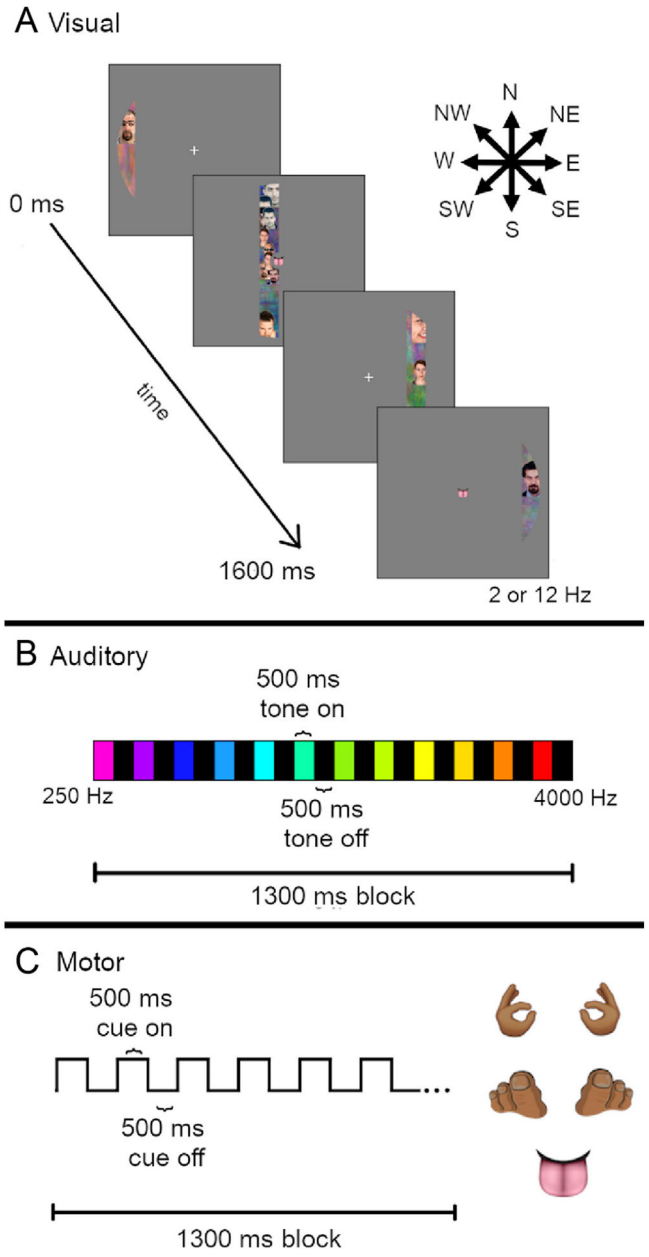

Fig. 1.

Population Receptive Field (pRF) mapping task. (A) Visual stimuli (dynamic sweeping bars, flickering at 2 or 12 Hz temporal frequency) were presented which traveled in one of eight directions (arrows, top right). Sweep duration was 16 s. (B) Auditory stimuli (pure tones, 250–4000 Hz) were presented in ascending or descending order during 13 s blocks. Tone duration was 500 ms with 500 ms of silence (scanner noise only) in between. (C) Motor task cue stimuli were presented at the center of the screen (i.e., fixation point, see A). Five different body part images were presented: left and right hands, left and right toes, and tongue. The participants' task was to tap the relevant body part in time with the cue presentation (500 ms on, 500 ms off, 13 s block duration).

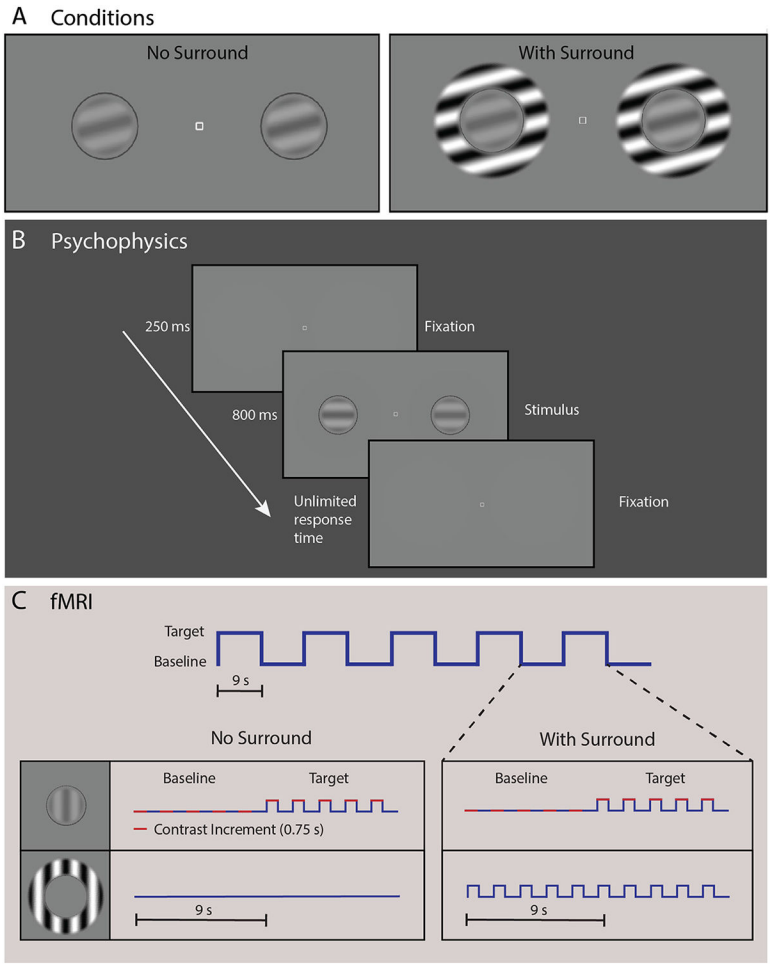

Fig. 2.

Contrast surround suppression (CSS) task. (A) Circular grating stimuli were present alone (left) or inside surrounding annular gratings (right; to induce the surround suppression illusion). Panel B shows the sequence for a single trial in our CSS psychophysical experiment. Participants were instructed to fixate on the center square and report which grating appeared ‘stronger,’ or higher contrast (left or right). In panel C, we illustrate the blocked experimental design for both the No Surround and With Surround conditions from our CSS fMRI task. Target and baseline stimuli were presented in 9 s blocks. Five stimulus presentations (trials) composed one block, with 5 pairs of target and baseline blocks composing one condition (90 s). In each trial, a contrast increment (red) was added at one of the two target locations. Surrounding stimuli (0% or 100% contrast for No Surround and With Surround, respectively) were held constant across both baseline and target blocks within each condition.

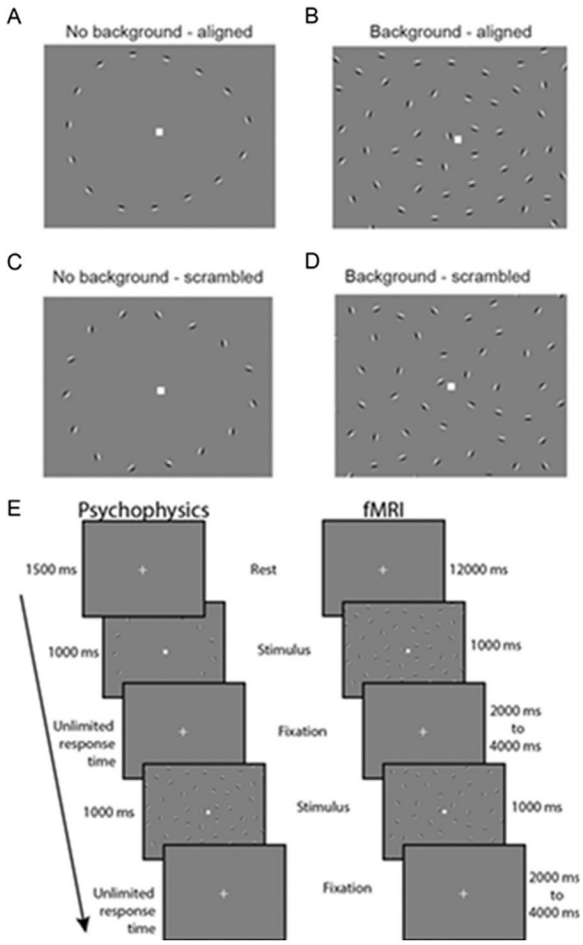

Fig. 3.

Contour object perception (COP) task. Panels A-D show example stimuli from 4 conditions: No background - aligned, Background - aligned, No background - scrambled, and Background - scrambled. Panel E (left column) shows the timing for a single trial from our COP psychophysical task. Participants were asked to report which direction an egg-shaped contour object pointed (left or right). In the right column, we show the timing for our COP fMRI paradigm, which included an initial 12 s rest period, followed by 1 s stimulus presentations with a jittered 2-4 s inter-stimulus interval.

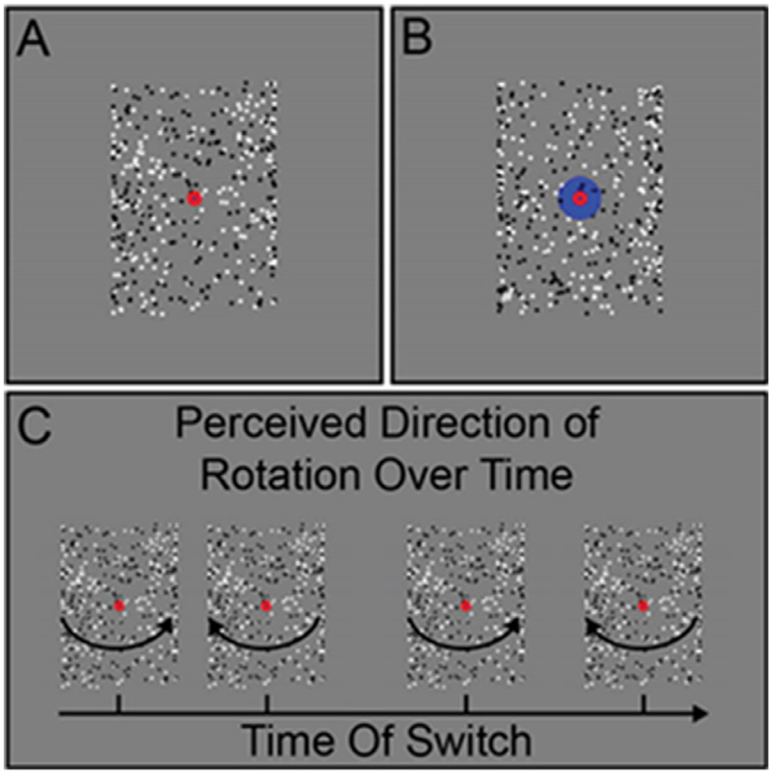

Fig. 4.

Structure-from-motion (SFM) task. Example stimuli for the real-switch task (A) and bi-stable task (B) conditions are shown. Panel C shows hypothetical examples of perceived switches in stimulus rotation direction across time during the bi-stable task.

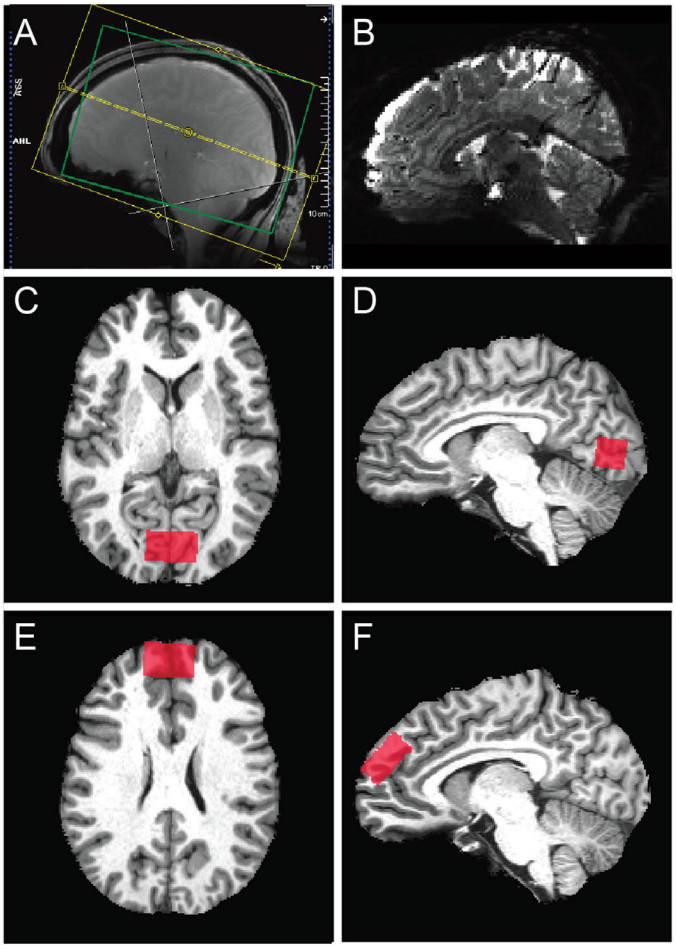

Fig. 5.

Functional MRI and MR spectroscopy acquisitions. A) Field of view (yellow) and adjustment volume (green) for fMRI. B) Example sagittal image from a GE EPI scan in a single participant. Panels C-F show example MRS volume placement (red) for occipital (C & D) and prefrontal (E & F) volumes-of-interest in axial (C & E) and sagittal (D & F) images from individual participants.

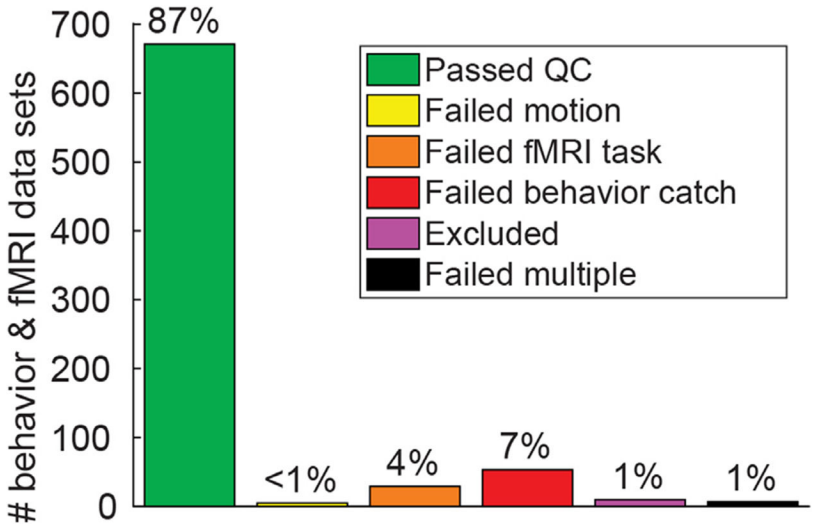

Fig. 6.

Behavioral and fMRI data quality. Chart shows the number and percentage of behavioral (psycho-physics) and fMRI data sets (not unique individuals) that passed or failed various data quality checks across 4 experiments (pRF, CSS, COP, & SFM).

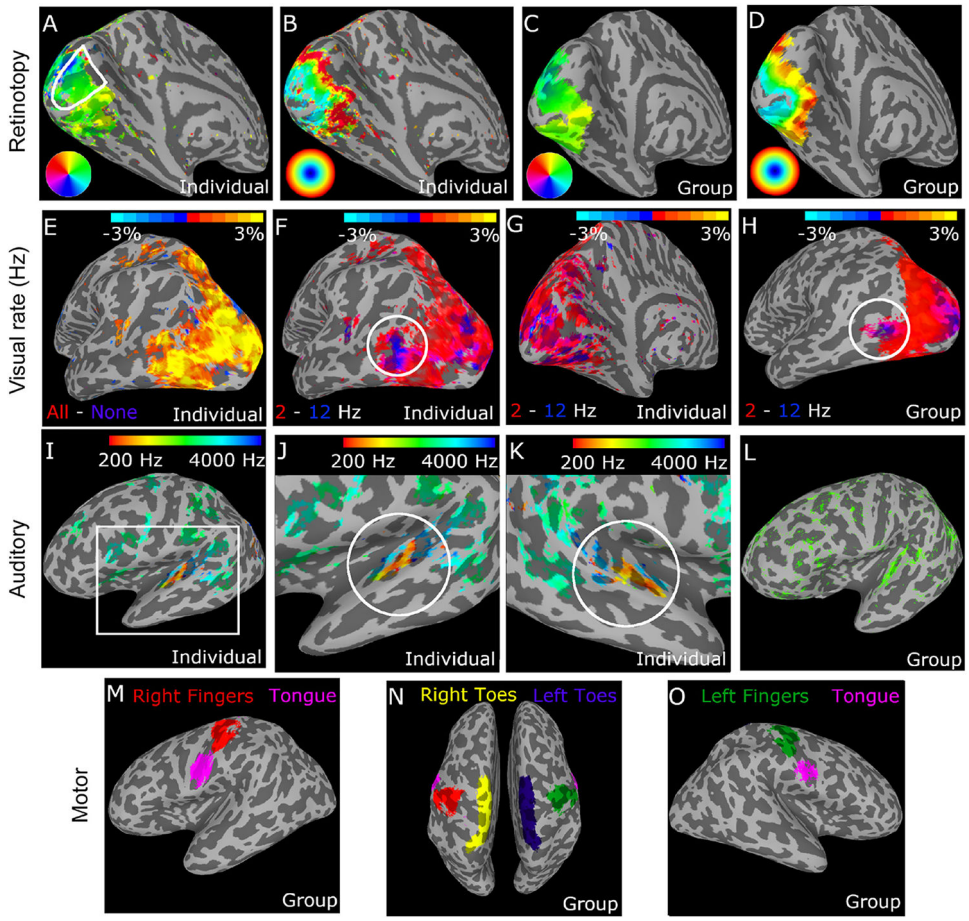

Fig. 7.

Results from the pRF fMRI task. Top row shows retinotopic fMRI results from the sweeping bars paradigm. Polar angle (A) and eccentricity (B) maps are shown from a single participant, as well as from a group of $n = 49$ controls (C & D). Color maps indicate retinotopic selectivity (e.g., right visual field locations are represented in the left hemisphere). Primary visual cortex is outlined in white in A. In the second row, responses to visual stimuli presented at 2 vs. 12 Hz were compared, to examine temporal frequency selectivity. Panel E shows response to all visual stimuli - none in 1 participant, F & G show 2 Hz - 12 Hz contrast from the same participant (lateral and medial views, respectively). Panel H shows the 2 Hz - 12 Hz contrast from a group of $n = 49$ controls. White circles in F & H indicate human MT complex (hMT+), a region selective for high temporal frequency stimuli (blue) in the lateral occipital lobe. Third row shows tonotopic fMRI responses to the auditory sweep stimuli. Panels I, J, & K show individual tonotopic responses in left and right hemispheres from a single participant, L shows data from a group of $n = 49$ controls. Color bar indicates voxel peak auditory frequency selectivity, from a Fourier analysis. White circles in J & K highlight auditory core regions on Heschl's gyrus. Note that spurious regions of activation outside of auditory cortex are present (e.g., central sulcus) due to the accidental confound of having 13 s blocks for both motor and auditory tasks. Figures in the bottom row (panels M, N, & O) show regions with selective fMRI responses during the motor tapping task from a group of $n = 49$ controls. Colors indicate selectivity for

different body parts. The relative position of different body part ROIs follows the expected ‘homunculus’ pattern in the region of the central sulcus. ROIs were defined using a contrast between the body part of interest and all other body parts. Voxels are included in the group level ROI if they were included in the individual level ROI for > 50% of participants.

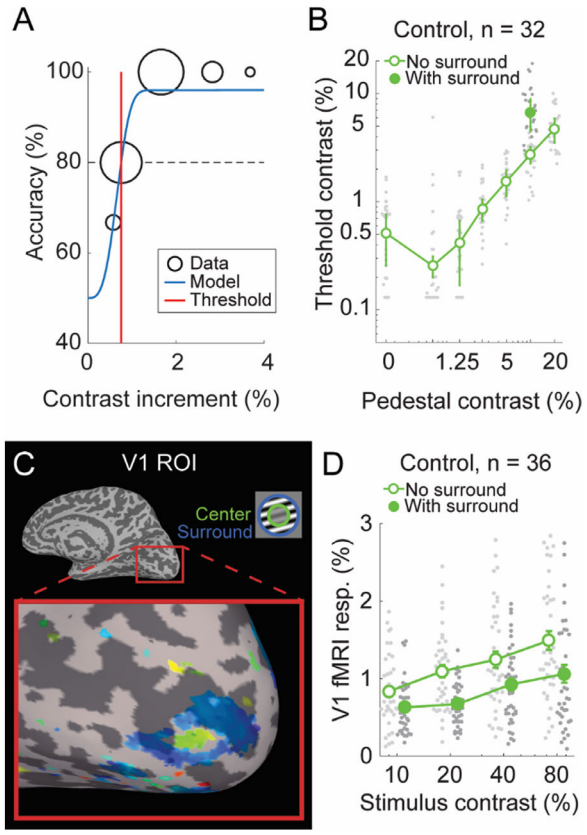

Fig. 8.

CSS task results. A) Example psychometric data from a single pedestal contrast condition in one participant. Data (black, size = # of trials) were fit with a Weibull function (blue) to obtain a discrimination threshold (red) at which stimulus contrast could be perceived with 80% accuracy (dashed line). B) Group threshold-versus-contrast data for $n = 32$ control participants in 8 different stimulus conditions (7 pedestal contrasts [x-axis], plus 10% pedestal with surround [filled circle]). These data show the expected 'dipper' function, with thresholds in the 0.6% pedestal condition being lower than for detection (0% pedestal). Gray dots show individual data points, green dots show group geometric means, error bars show median absolute deviation. C) Functional localizer data from the CSS fMRI task in a single participant. A region of primary visual cortex is highlighted, which shows spatial selectivity for the center stimulus region (green) versus the surround (blue). Color indicates the phase of the fMRI response from a Fourier analysis (Engel, 1997). D) CSS fMRI responses from V1 center-selective ROIs in the no surround (open, offset left) and with surround (closed, offset right) conditions across 4 pedestal contrasts, in a group of $n = 36$ controls. Gray dots show individual data points, green dots show group means, error bars show S.E.M.

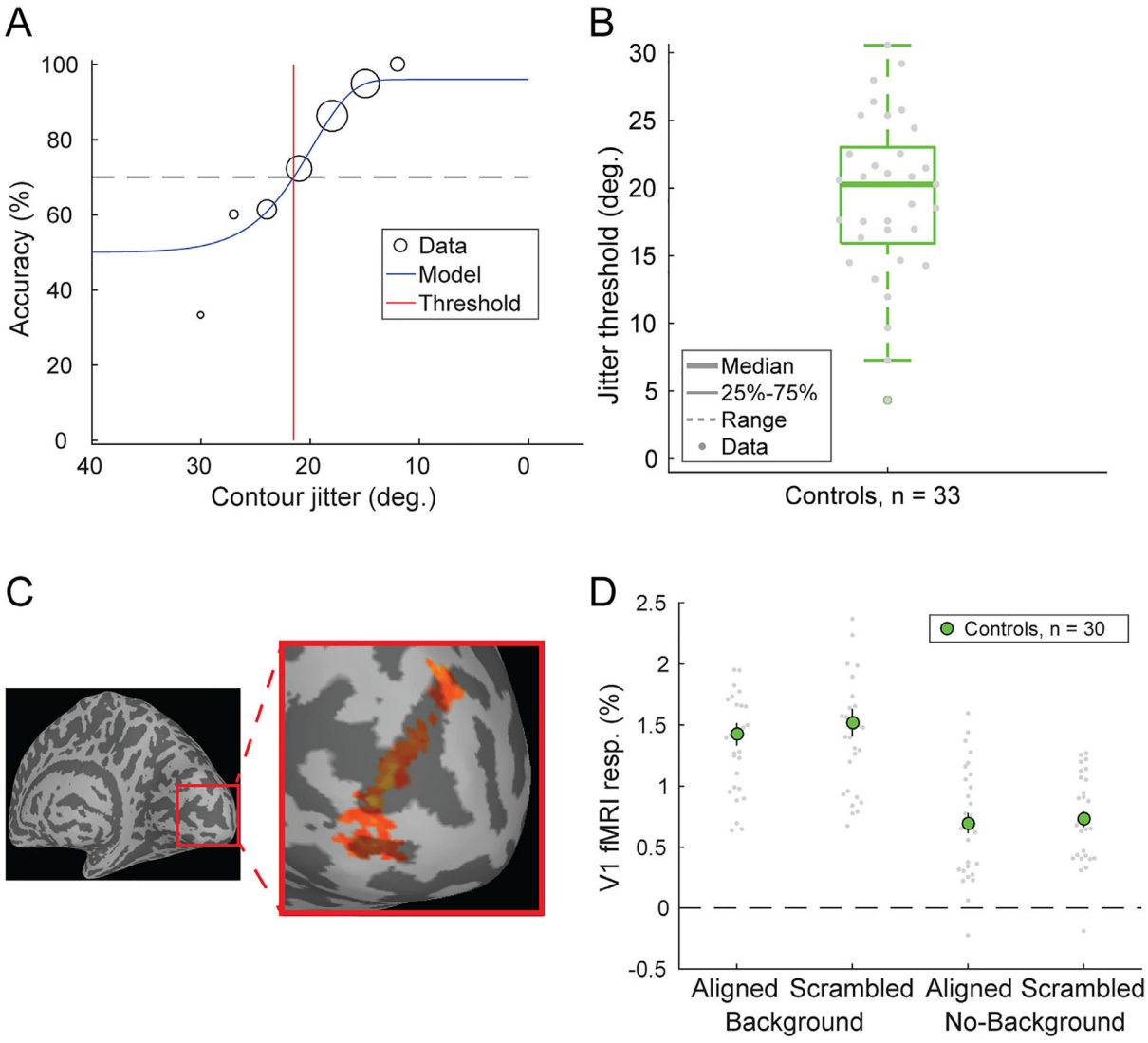

Fig. 9.

COP task results. A) Example COP psychophysical data (black, size = # of trials) from a single participant were fit with a Weibull function (blue) to obtain a jitter threshold (red), reflecting 70% contrast discrimination accuracy (dashed line). B) Jitter thresholds for $n = 33$ controls. Thick line shows median, box shows 25-75%, whiskers show 1.5 x interquartile range, gray dots show individual data points. C) COP functional localizer data from area V1 in the right hemisphere from an example participant. Color indicates statistical significance from a Fourier analysis (Engel, 1997) showing voxels selective for the COP localizer stimulus > blank. D) COP fMRI responses from retinotopic contour ROIs in area V1 across 4 stimulus conditions in a group of $n = 30$ controls. The presence of background stimuli increased the fMRI response (as expected, with more stimuli on the screen), whereas we saw little effect of contour alignment in the V1 fMRI response.

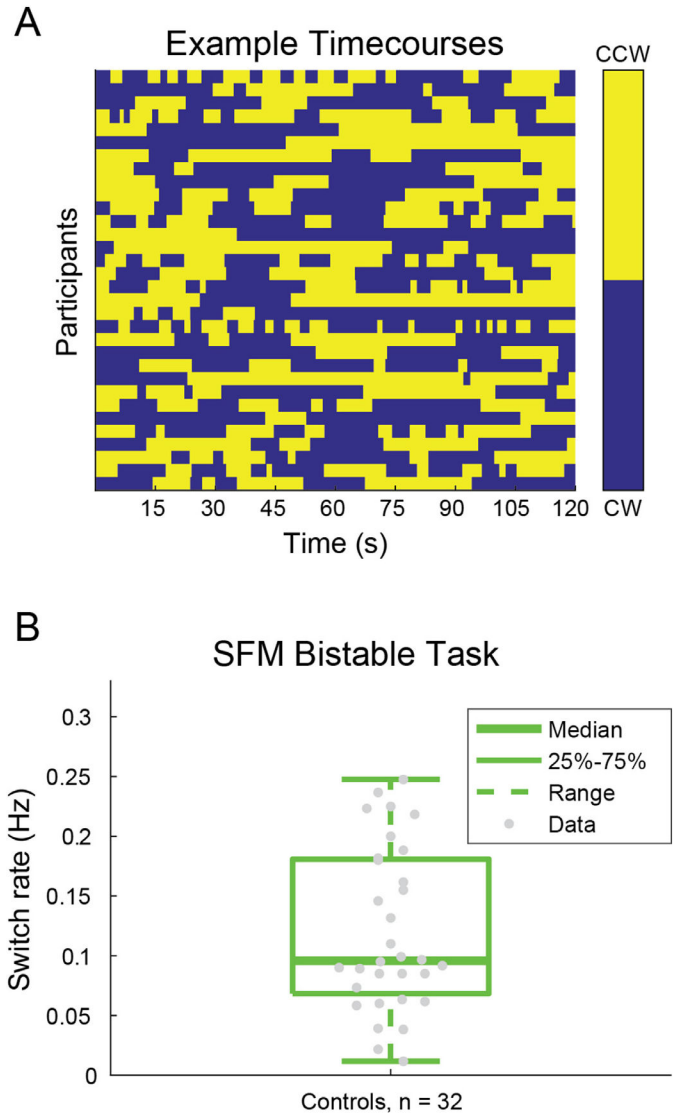

Fig. 10.

SFM results. A) Example behavioral response time courses from the bi-stable task, showing perceived switches between clockwise (CW, blue) and counterclockwise (CCW, yellow) rotation in depth. Data from a single 120 s block are shown for $n = 32$ control participants. B) Bi-stable switch rates from the same group of participants. Thick line shows group median, box shows 25-75%, whiskers show 1.5 x interquartile range, dots show individual participants.

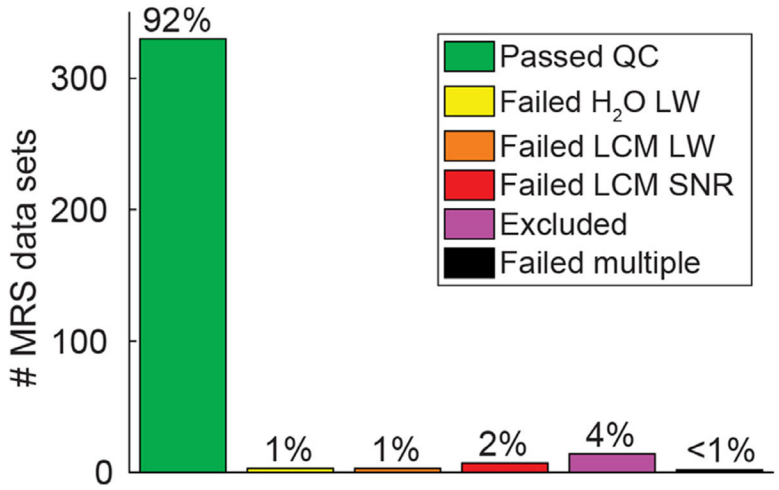

Fig. 11.

MRS data quality. Chart shows the number and percentage of MRS data sets (not unique individuals) that passed or failed various data quality checks across 2 VOIs (OCC and PFC). H_2O LW = water linewidth, LCM LW = LCModel linewidth, LCM SNR = LCModel signal-to-noise ratio.

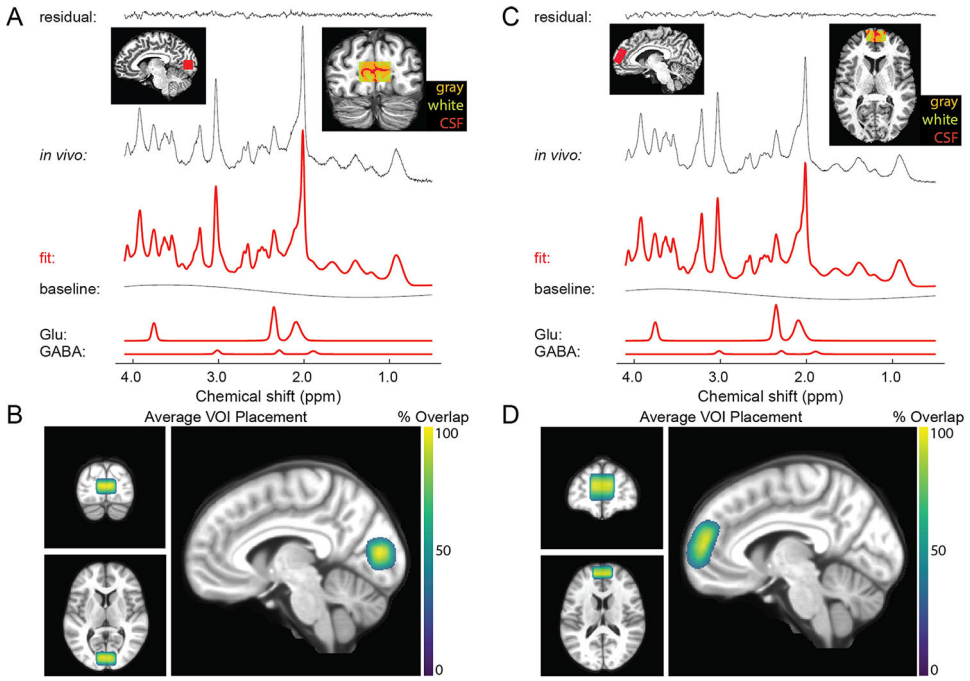

Fig. 12.

Example MRS spectra and average VOI positions. A) OCC spectrum from a single participant (black) fitted with LCModel (red). Top left inset shows a sagittal view of OCC VOI placement. Top right inset shows a coronal view of the OCC VOI, with gray matter (orange), white matter (yellow), and cerebrospinal fluid (CSF, red) highlighted. Bottom rows show glutamate (Glu) and GABA components, as fitted by LCModel. B) Average OCC VOI placement across $n = 193$ data sets (including repeats). Color shows overlap across participants. VOI masks were transformed from individual to MNI space, and thresholded at 30% overlap. C and D show the same as A & B, but for the PFC VOI ($n = 147$ data sets in D).

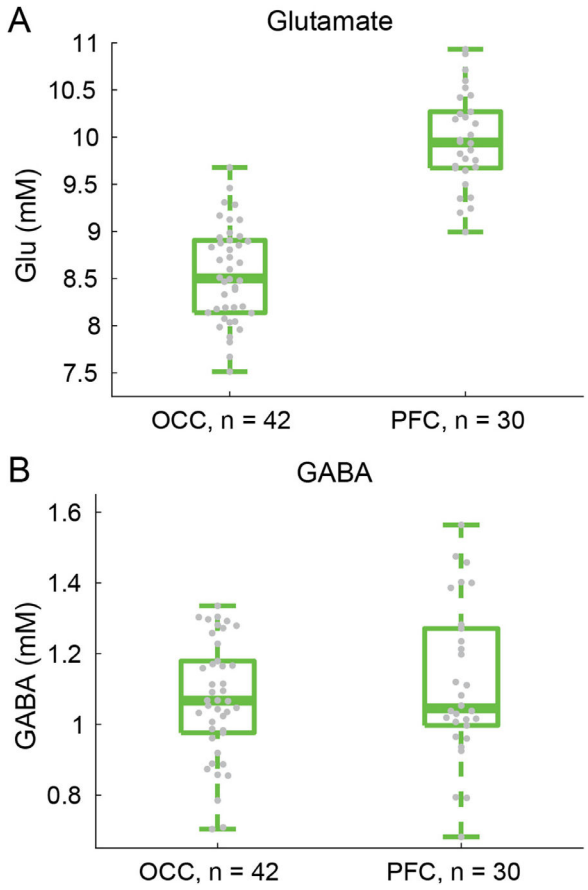

Fig. 13.

MRS results showing (A) glutamate and (B) GABA concentrations in OCC and PFC, from a group of $n = 42$ & 30 participants, respectively. Fewer PFC data sets were collected due to a delay in hardware availability, as noted in the Methods. Thick lines show group medians, boxes show 25-75%, whiskers show 1.5 x interquartile range, gray dots show data points from individual participants.

Table 1

Participant demographics, cognitive, and symptom measures. Data are presented as mean (standard deviation), unless otherwise noted. Racial and ethnic designations (as defined by the National Institute of Health) are abbreviated as follows: A = Asian or Pacific Islander, B = Black (not of Hispanic origin), H = Hispanic, N = Native American or Alaskan Native, W = White (not of Hispanic origin), M = More than 1 race or ethnicity, or other. Visual acuity was assessed with a Snellen eye chart (Snellen, 1862); the decimal fraction is reported (e.g., 0.5 indicates 20/40). Visual contrast sensitivity was assessed with the Mars Letter Contrast Sensitivity test (Arditi, 2005). Estimated IQ was assessed using the Wechsler Adult Intelligence Scale (WAIS-IV; Wechsler 2008). BACS = Brief Assessment of Cognition in Schizophrenia, Z-score (Keefe et al., 1999), BPRS = Brief Psychiatric Rating Scale Total Score (Ventura et al., 2000), SGI = Sensory Gating Inventory (Hetrick et al., 2012), SPQ = Schizotypal Personality Questionnaire (Raine, 1991), PID-5 psychoticism = psychoticism factor from the Personality Inventory for DSM-5 (Krueger et al., 2012), SANS = Scale for the Assessment of Negative Symptoms Total Global Score (Andreasen, 1982), SAPS = Scale for the Assessment of Positive Symptoms Total Global Score (Andreasen, 1984). Diagnoses were based on the Structured Clinical Interview for DSM-IV-TR disorders (SCID; First 1997). Data collected at repeat scans were not included here. For the relative group, the number of related probands with a particular psychotic disorder diagnosis is listed in square brackets. The statistics column shows the test statistic and *p*-value for differences across all three groups in each measure. For measures where normality and / or homogeneity of variance were not observed, non-parametric Kruskal-Wallis tests (X^2-values) were used in place of analyses of variance (*F*-values).

	Controls, n = 43	**Relatives, n = 44**	**PwPP, n = 66**	**Statistics**
Age (years)	37.8 (12.2)	43.5 (13.0)	38.4 (11.6)	$F_{2,150} = 3.0, p = 0.054$
Sex assigned at birth	23 F, 20 M	30 F, 14 M	31 F, 35 M	$X^2_2 = 4.8, p = 0.09$
Race / ethnicity (%; A / B / H / N / W / M)	2.3 / 4.7 / 0 / 0 / 90.7 / 2.3	2.3 / 4.5 / 0 / 0 / 88.6 / 4.5	4.5 / 15.2 / 3.0 / 0 / 74.2 / 3.0	-
Education (years)	16.2 (2.1)	15.5 (2.1)	14.2 (2.3)	$F_{2,150} = 11.5, p = 2 \times 10^{-5}$
Visual acuity (decimal fraction)	0.95 (0.27)	0.97 (0.31)	0.95 (0.56)	$F_{2,99} = 0.02, p = 1.0$
Visual contrast sensitivity	1.84 (0.06)	1.80 (0.05)	1.79 (0.07)	$F_{2,149} = 6.3, p = 0.003$
Estimated IQ	108 (9.3)	104 (9.8)	97 (10.7)	$F_{2,150} = 16.0, p = 5 \times 10^{-7}$
BACS	0.37 (0.54)	0.01 (0.74)	−0.66 (0.69)	$F_{2,149} = 33.3, p = 1 \times 10^{-12}$
BPRS	26.7 (3.4)	30.8 (6.8)	42.2 (10.7)	$X^2_2 = 58.7, p = 2 \times 10^{-13}$
SGI	35.5 (19.6)	50.5 (31.5)	69.3 (29.5)	$X^2_2 = 34.5, p = 3 \times 10^{-8}$
SPQ	8.1 (8.2)	14.9 (13.3)	30.4 (15.0)	$X^2_2 = 56.7, p = 5 \times 10^{-13}$
PID-5 psychoticism	0.27 (0.28)	0.38 (0.40)	1.16 (0.64)	$X^2_2 = 64.9, p = 8 \times 10^{-15}$
SAPS	-	-	4.71 (4.30)	-
SANS	-	-	6.05 (3.88)	-
Diagnoses[of related proband]				

	Controls, n = 43	Relatives, n = 44	PwPP, n = 66	Statistics
Schizophrenia	0	0 [23]	36	-
Schizoaffective	0	0 [8]	10	-
Bipolar disorder	0	1 [13]	20	-
Other (e.g., MDD)	3	18	0	-
None	40	25	0	-
Days between 3 T and 7 T scans	102 (96)	232 (264)	241 (311)	-
# of 7 T return visits	10	0	39	-
Days between 7 T repeat scans	381 (306)	-	253 (312)	-

Table 2

Number of data sets collected for each experiment. Values are reported as: unique individuals (*repeated data sets*). CSS = contrast surround suppression, COP = contour object perception, SFM = structure from motion, pRF = population receptive field, fMRI = functional magnetic resonance imaging, MRS = magnetic resonance spectroscopy, OCC = occipital cortex, PFC = prefrontal cortex

Data type	Experiment	Controls, n = 43	Relatives, n = 44	PwPP, n = 66
Psychophysics	CSS	34 (*9*)	44 (*0*)	66 (*39*)
	COP	42 (*9*)	44 (*0*)	66 (*39*)
	SFM	43 (*10*)	44 (*0*)	65 (*39*)
fMRI	pRF	42 (*10*)	40 (*0*)	53 (*33*)
	CSS	33 (*10*)	39 (*0*)	52 (*32*)
	COP	35 (*10*)	39 (*0*)	48 (*29*)
MRS	OCC	43 (*10*)	42 (*0*)	62 (*36*)
	PFC	21 (*10*)	38 (*0*)	50 (*33*)